Double-Double laminates - A review on the status quo in spring 2024

Erik Kappel and Stephen W. Tsai*

June 12, 2024

*Corresponding author: Dr.-Ing. Erik Kappel, erik.kappel@dlr.de, Composite design department (FLB), Institute of Lightweight Systems (SY), Braunschweig, Germany

Download from DLR ELIB:
https://elib.dlr.de/204753/

DOI:
https://doi.org/10.57965/g2cb-8t21

The article summarizes recent activities in context of the Double-Double laminate family. The article provides brief summaries of published numerical and experimental studies. Small-scale manufacturing demonstrators are presented in addition, which highlight DD's unique manufacturing opportunities. The article is closed by a summary, which outlines composite-material types that have been examined experimentally in the DD context.

Contents

Abbreviations

Abbreviation	meaning
BB	building block
CAI	Compression after impact
CFRP	Carbon-fiber-reinforced plastics
CLT	Classical laminate theory
CTE	Coefficient of thermal expansion
DD	Double-Double
ENF	End-notched flexure
FAW	Fiber areal weight
FE	Finite element
FHT/FHC	Filled hole tension/ compression
GFRP	Glass-fiber-reinforced plastics
Metalite	A particular laminate group with 8-ply BB
NCF	non-crimp fabric
NCTE	Negative coefficient of thermal expansion
OHT/OHC	Open hole tension/ compression
Quad	Conventional laminate, composed of $0°, 45°, -45°, 90°$ plies
SLS	Single-lap shear
SSBT	Single-shear, single-fastener bearing tension
ST	Strain threshold
UD	Unidirectional

1 *Motivation*

Double-Double laminates attracts the aerospace composite sector increasingly, in research groups and in industry. DD laminates show opportunities in laminate design context and especially in the manufacturing. However, getting an overview on '*What has already been done for DD?*' is difficult. Therefore, this article aims to summarize the recent DD activities, which have been published until January 2024. The two books, shown in Figure 1, summarize relevant activities. The present article outlines numerical and experimental studies and provides selected manufacturing samples, which feature DD's unique opportunities.

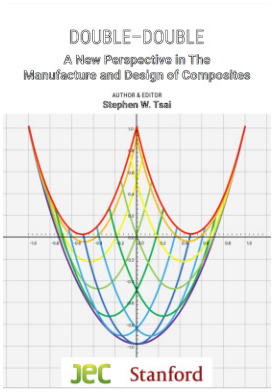

(a) 2022 @ JEC, Paris

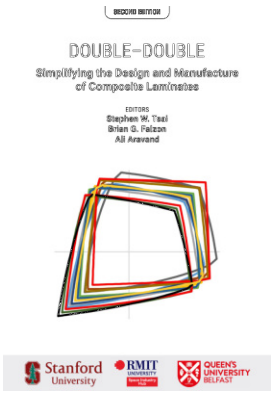

(b) 2023 @ ICCM, Belfast

Figure 1: Recent DD book publications

2 *A brief introduction to Double-Double laminates*

Laminate in aerospace applications often feature the four ply orientations $0°$, $\pm 45°$ and $90°$. Those laminates are hereafter denoted as 'conventional' laminates, which are often denoted 'Quad' [1] in short. Conventional laminate are usually symmetric and balanced, while certain ply-fraction thresholds are defined in practice.

Double-Double laminates is 'just' another group of laminates. A DD laminate features a sequence of sub-laminates, which represent identical four-ply building blocks. The number of repetitions r describes how many BBs are stacked. Symmetry requirements omit! The four-ply building block is defined by the two ply angles φ, Ψ, which are present with positive and negative sign. Thus, a BB is balanced per definition. The exact stacking sequence within the BB is not prescribed. One finds $[\pm\varphi, \pm\Psi]_{rT}$ as a typical laminate description, in which T denotes 'total'. The previous DD layup refers to a non-crimp-fabric (NCF) manufacturing scenario, in which the BB is composed of two 'doubles'. Therein, one double represents a two-ply (bi-axial) NCF, with fiber orientations in $+\varphi$ and $-\varphi$, for example [19]. In this scenario, it is the idea, to compose a single BB from two different bi-axial NCF materials.

However, DD laminates are not limited to the NCF scenario. A DD laminate can be excellently manufacturing from state of the art unidirectional (UD) plies, in a dry-fiber placement or a prepreg process. Most of the examples shown in Section 5 are actually made from conventional prepregs available today. In case, laminates made from single UD plies are in focus, it is recommended to substitute the previous '$\pm$' notation, by a ply-based one. BB stackings $[\varphi, -\varphi, \Psi, -\Psi]$ or $[\varphi, -\Psi, -\varphi, \Psi]$ are valid selections. A recent study [7] shows, that the sequence $[\varphi, \Psi, -\Psi, -\varphi]$ does not lead to DD homogenization effects, which is explained hereafter. Thus, it recommended not to use

Note, that the notation $[\pm\Phi, \pm\Psi]_{rT}$ is frequently used as well. For consistency purposes, φ and Ψ are used in this article.

the $[\varphi, \Psi, -\Psi, -\varphi]$ for the BB.

Classical-laminate-theory (CLT) (see [29]) is usually used for composite design tasks for conventional laminates in practice. The $[ABD]$-matrix is the core of the CLT, interrelating in-plane loads (N_x, N_y, N_{xy}) and bending moments (M_x, M_y, M_{xy}) with mid-plane strains $(\varepsilon_x, \varepsilon_y, \gamma_{xy})$ and curvatures $(\varkappa_x, \varkappa_y, \varkappa_{xy})$. The sub matrices $[A]$, $[B]$ and $[D]$ have different units N/mm, N, Nmm, respectively.

Analytical calculations in DD context are often presented with a slightly modified description, which can be deduced from the conventional CLT version. DD laminates are usually presented with thickness-normalized matrices

$$[A^*] = [A]/t, \quad [B^*] = 2[B]/t^2, \quad [D^*] = 12[D]/t^3.$$

This is not a necessary change, but it offers some advantageous. $[A^*], [B^*]$ and $[D^*]$ have all the same units N/mm^2 for example. The adapted CLT formulation is developed as follows:

$$\underbrace{\begin{pmatrix}\{N\}\\ \{M\}\end{pmatrix} = \begin{bmatrix}[A] & [B]\\ [B] & [D]\end{bmatrix} \cdot \begin{pmatrix}\{\varepsilon^0\}\\ \{\varkappa\}\end{pmatrix}}_{\text{CLT}} \rightarrow \underbrace{\begin{pmatrix}\{\sigma^0\}\\ \left\{\sigma^f\right\}\end{pmatrix} = \begin{bmatrix}[A^*] & [B^*]\\ 3[B^*] & [D^*]\end{bmatrix} \cdot \begin{pmatrix}\{\varepsilon^0\}\\ \left\{\varepsilon^f\right\}\end{pmatrix}}_{\text{Normalized, see Tsai and Melo [22]}}$$

with $\{\sigma^0\} = t_{lam} \cdot \{N\}$, $\left\{\sigma^f\right\} = \frac{t_{lam}^2}{6} \cdot \{M\}$ and $\left\{\varepsilon^f\right\} = \frac{t_{lam}}{2} \cdot \{\varkappa\}$. Homogenization is the key feature of DD laminates. The process is linked to the number of building-block repeats, described by the parameter r. One observes the r-dependencies. $[B^*] \propto 1/r$ and $D_{16,26} \propto 1/r^2$. More important, one observes

$$[D^*] = \begin{bmatrix} \cancel{f(r)} & \cancel{f(r)} & \frac{1}{r^2} \cdot (\ldots) \\ \cancel{f(r)} & \cancel{f(r)} & \frac{1}{r^2} \cdot (\ldots) \\ \frac{1}{r^2} \cdot (\ldots) & \frac{1}{r^2} \cdot (\ldots) & \cancel{f(r)} \end{bmatrix} \quad . \tag{1}$$

which is an important finding in context of buckling analysis. All relevant bending-stiffness-matrix coefficients for buckling of plates (D_{11}, D_{12}, D_{22} and D_{66}) are found independent from r. This, allows for simplification for buckling (see [10]), as stacking sequence discussion diminish. Homogenization is driven by building block repeats. The matrix population of a homogenized DD laminate approaches the population of an isotropic media, as shown on the right. Thus, the complex couplings between strain and curvature do not exist. Bending-twist coupling, driven by the D_{16}, D_{26} reduced diminished proportional with $1/r^2$.

$$[ABD]_{DD}^{r\to\infty}: \begin{bmatrix} \bullet & \bullet & 0 & \approx 0 & \approx 0 & \approx 0 \\ \bullet & \bullet & 0 & \approx 0 & \approx 0 & \approx 0 \\ 0 & 0 & \bullet & \approx 0 & \approx 0 & \approx 0 \\ \approx 0 & \approx 0 & \approx 0 & \bullet & \bullet & \approx 0 \\ \approx 0 & \approx 0 & \approx 0 & \bullet & \bullet & \approx 0 \\ \approx 0 & \approx 0 & \approx 0 & \approx 0 & \approx 0 & \bullet \end{bmatrix}$$

Finding a DD substitute for conventional laminate is usually possible, despite for more-orthotropic laminate as outlined the in the next section. For regular case, on can setup a simple optimization scheme with the objective function being defined as:

$Min : \sum |A^*_{ij,DD} - A^*_{ij,Quad}|$ for $i, j = 1, 2, 6$. A similar formulation is conceivable which focuses on the bending stiffness properties (D^*_{ij}). When the ply-stiffness matrix $[Q]$ and a normalized laminate-stiffness matrix $[A]$ are known. the corresponding BB ply angle of a DD equivalent can be analytically determined using invariants and normalizes lamination parameters.

Cunha et al. [12] outline the procedure. The most simple approach neither need optimization nor invariants and lamination parameters. One can simply determine $\sum |A^*_{ij,DD} - A^*_{ij,Quad}|$ for all conceivable angle combinations φ, Ψ. Afterwards, the minimum value is identified, and the corresponding φ, Ψ combination is picked. A 1° discretization forφ and Ψ, this refers to only 4186 calculations, when design-space symmetry is considered.

Tsai's Modulus shall be highlighted here, which has been presented by a group of renowned researchers in [37] in 2020. Tsai's Modulus is intensively used in DD context in multiple publications. A recent study adds that Tsai's Modulus, is particular case of a parametric invariant description.

More-orthotropic DD laminates

In today's laminate-design guidelines for conventional laminates in aerospace, one finds limits for the ply-orientation fraction, of the $0^\circ, \pm 45^\circ, 90^\circ$ plies.

An upper threshold of around 60% is considered for the fraction of 0° plies in a laminate. This, high value is utilized when more-orthotropic laminates $(E_x >> E_y)$ are required. One find those in inner flanges of fuselage frames and also in upper and lower wing covers (see $[0_3/90/\pm 45/0_2/\pm 45]_{2S}$ Cunha [12]). A DD building block is defined by φ and Ψ. To exclude the trivial solution of a UD laminate, it is essential to realize $(\varphi \neq \Psi)$. Thus, 50% 0° plies in the building block is the upper threshold. This implies, that an DD equivalent for a conventional more-orthotropic laminate cannot be found, when the 0° fraction in the conventional laminate is higher than 50%. Figure 2 visualizes this based on lamination parameter space. The black region refers to DD laminates. The red region refers to Quad, laminates, while a minimum ply-orientation fraction of 8% for the $0^\circ, \pm 45^\circ, 90^\circ$ are considered. The upper right region of the red area refers to more-orthotropic laminates.

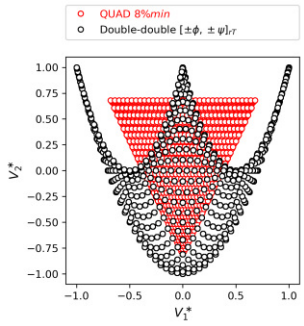

Figure 2: Laminate parameters V_2^* over V_1^* for DD and for Quad.

Note, that Shrivastava et al. [13] and Cunha et al.[12], for example, examine $[\pm 0, \pm 54]$ and $[\pm 0, \pm 50]$ DD configurations, respectively.

An analytical study in ongoing, which examines whether more orthotropic DD laminates can be achieved by adding an single or multiple 0° layer(s) to the DD building block, such as $[0_i, \pm\varphi, \pm\Psi]$. The analysis shows that the initial DD design space can be shifted (Figure 2), allowing for more-orthotropic DD laminates. However, the important DD property, of r-independence of the coefficients of the (see Equation 1), diminishes for 5- or 6-ply building blocks.

When additional 0° layers are added to the BB, the denomination as DD would be misleading. Something like $DD0_i$ would be more precise and therefore recommended.

3 *Experimental studies*

CAI

Kappel et al. performed a study focused on the CAI behavior of DD laminates [11]. Aside from constant thickness sample, with 16 and 32 plies, tapered samples were examine, which feature a transition region from 16-32. All samples are made from medium grade M21E/IMA UD prepreg. The DD laminates feature the $[\pm 22.5, \pm 67.5]$ building block. The DD laminate philosophy leads to difference how thickness transitions are designed. Quad laminates usually show staggered single-ply drop offs along a ramp and continuous cover plies. DD laminates show a stair-shaped discrete steps, with full BB drop offs and no cover plies. Figure 3 shows section cuts of a tapered DD and a Quad sample, to highlight the different inner laminate architecture. The Quad samples feature conventional ply orientations.

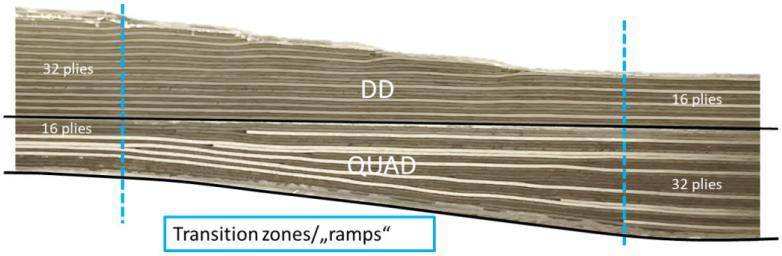

Figure 3: Laminate ramps (32-to-16 plies) for DD (top) and for Quad

The open building-block drop offs / run out are potentially critical regions. Those can eventually promote crack initiation and crack propagation underneath transition zone. Experimental evidence has not been available.

Figure 4 summarizes all tested scenarios. Those tests were executed for DD and Quad laminates.

Similar risk can be anticipated for fatigue load scenarios!

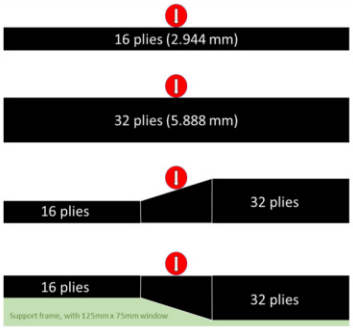

Figure 4: Examined impact cases. The third and fourth case are denoted as 'ramp' and 'ramp-down', respectively.

The constant-thickness samples were tested with five discrete energy levels. The tapered samples were tested at 50 J only, with five samples per configuration. Figure 5 shows total delamination areas

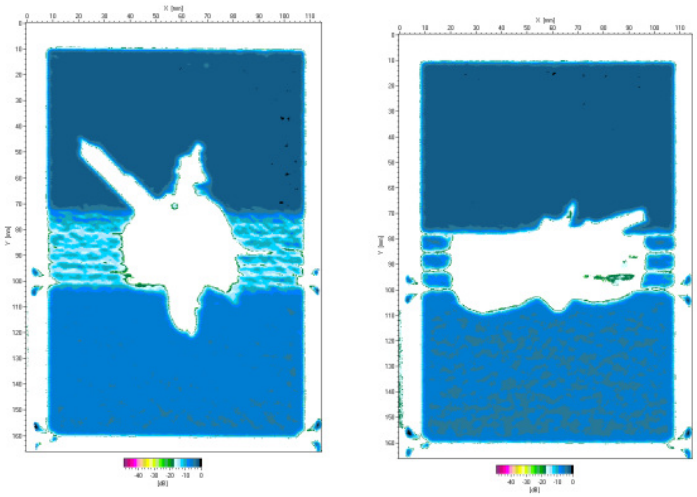

(a) QUAD (b) DD

Figure 5: Delamination area comparison

for the tapered samples. The image clearly shows that the different laminate architecture affects the delamination behavior. The US scans show higher delamination-area widths for the DD samples, which can be seen when comparing in Figure 5. However, the depth of delaminations could not be clearly assessed based on the available US-scans. Thus, the compression tests after impacting were particularly interesting in order to check the correlation of damage-width and strength. Figure 6 shows the force-displacement graphs

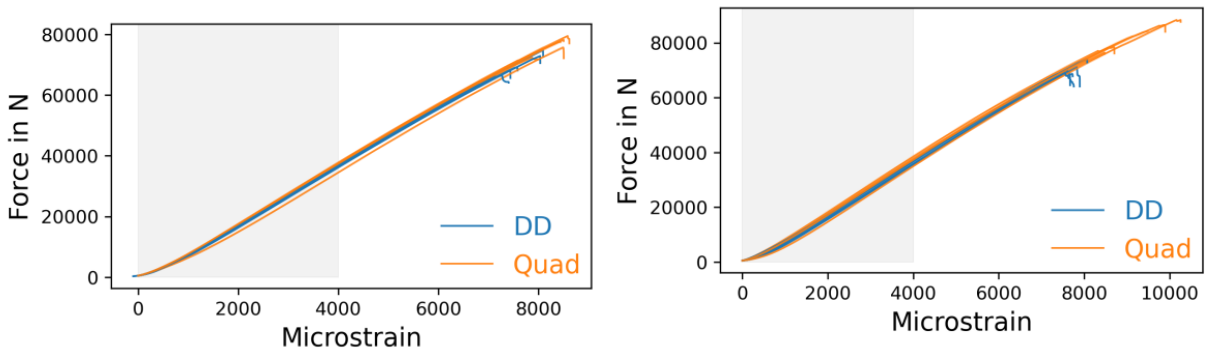

(a) 'ramp' case (b) 'ramp-down' case

Figure 6: Force-displacement graphs for Quad and DD sample after impacting the ramp region with 50 J

from the compression tests. Both graphs show that the both DD and Quad will have very similar stiffness. For the 'ramp' case, overlaying failure regions are observed for DD and Quad, with failure strains

between 7000-9000 microstrain. For the 'ramp-down' scenario, the compression tests show two main things. DD shows less scattering, but slightly lower failure strains at around 8000 microstrain. Single Quad samples show failure strains at around 10000 microstrain. A correlation between compressive strength after impact and the total delamination area or width could not be substantiated. Up to usually exploited strain levels of 5000 microstrain, the sample do not show remarkable differences in the force-displacement graphs.

Tension/Compression and OHT/OHC

Open-hole-tension for has been examined by Kappel et al. [16]. Figure 7 shows selected samples prior testing.

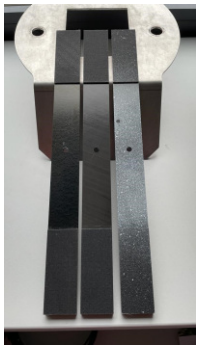

Figure 7: DD OHT samples prior testing [16]

The OHT tests have been executed conform to norm AITM 1-0007 [36]. The study examine low- (8552/IM7) and an interleaf-toughened medium grade prepreg (M21/IMA). A QI and a more orthotropic conventional laminate serve as baseline. DD equivalents were determined and manufactured. The testing was accompanied by full-field, high resolution optical measurement and corresponding FE studies, to asses the match between experiment and simulation models. Figure 8 summarizes the executed tension testing. The assessment of the optical scans is ongoing and the corresponding FE models is ongoing.

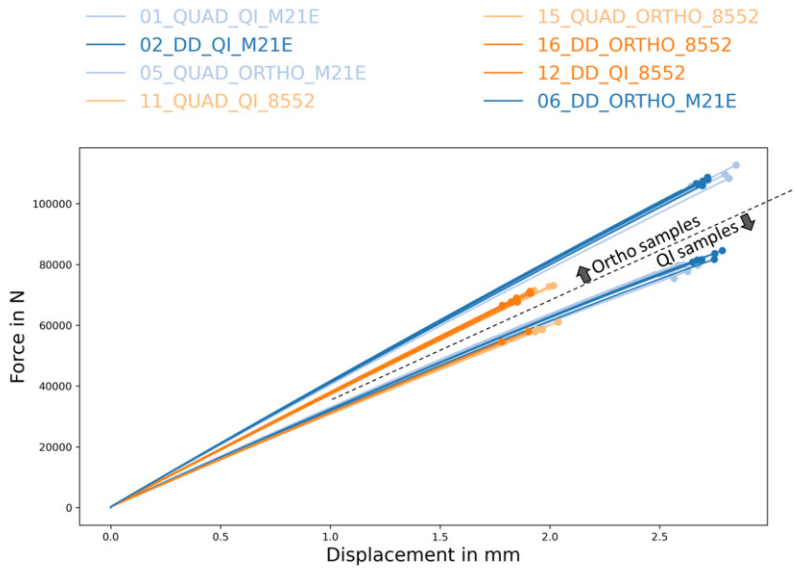

Figure 8: OHT Study at a glance [16]

Seneviratne et al. [18] examined Tension/Compression and OHT/OHC and also open-hole compression. The test focus was on more-orthotropic

20-ply laminates. The examined Quad laminate has a symmetric $[0_5, (\pm 45)_2, 90]_s$ stacking, which is a $(50\%, 40\%, 10\%)$. The DD competitor has a $[\pm 0, \pm 50]_{5T}$ stacking. All samples feature Toray's T700 fibers. Figure 9 summarizes the test results. Both strength and modulus comparisons show a high level of comparability. Obvious advantageous or disadvantageous for DD or Quad were not identified.

We thank Waruna Seneviratne, PhD. for providing the information on the executed tests.

MATERIAL SYSTEM	LAYUP	TEST METHORD	SPECIMEN NAME	MAX LOAD [lbf]	STRENGTH [ksi]	MODULUS I [Msi]	MODULUS II [Msi]	AVERAGE MODULUS [Msi]
Toray	DD	No Hole Compression	DD-Layup-NHC-1	16441	91.5	10.3	8.5	9.4
			DD-Layup-NHC-2	16480	91.3	9.5	9.4	9.4
	HARD		Hard-Layup-NHC-1	14819	82.4	9.4	9.8	9.6
			Hard-Layup-NHC-2	16168	91.7	9.6	9.3	9.4
	DD	No Hole Tension	DD-Layup-NHT-1	35945	200.7	9.5	9.6	9.6
			DD-Layup-NHT-2	35570	197.5	9.5	9.6	9.5
	HARD		Hard-Layup-NHT-1	38106	211.5	9.8	10.1	9.9
			Hard-Layup-NHT-2	37526	207.0	10.0	9.9	9.9
	DD	Open Hole Compression	DD-Layup-OHC-1	9562	53.5	9.8	8.7	9.2
			DD-Layup-OHC-2	10051	56.3	9.1	9.1	9.1
	HARD		Hard-Layup-OHC-1	9771	55.3	10.9	9.4	10.1
			Hard-Layup-OHC-2	9486	52.8	8.7	9.5	9.1
	DD	Open Hole Tension	DD-Layup-OHT-1	17909	100.0	9.7	9.4	9.5
			DD-Layup-OHT-2	18944	106.1	9.9	9.6	9.7
	HARD		Hard-Layup-OHT-1	17605	98.6	10.0	10.1	10.0
			Hard-Layup-OHT-2	17496	97.7	10.0	9.9	9.9

Figure 9: Result summary for tension, compression, OHT and OHC tests for Toray material, featuring T700 fibers.

Bearing, SSBT

Waruna Seneviratne and colleagues from National Institute for Aviation Research (NIAR), Wichita State University (WSU) tested DD laminates for their bearing response according to the ASTM D5961 [18]. Among other laminates, the study examines $[\pm 75, \pm 15]$ and $[\pm 0, \pm 15]$ samples. Figure 10 shows the tested samples. The tested samples were provided by Toray.

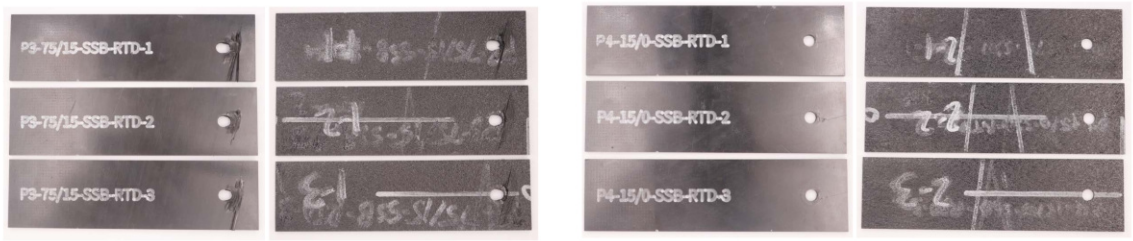

Figure 10: Single-shear, single-fastener bearing tension (SSBT) test samples

Fatigue

The fatigue behavior of DD laminates has attracted comparably little attention. Figure 11 shows supposedly the only published testing activity, which has been presented recently at JEC 2024 [35]. The tested samples feature Chromarat's 0/50 bi-angle dry-fiber C-Ply™material, which features Toray's T700 fibers (2 layers with 50 g/m^2 FAW each). The tested samples are made in an vacuum infusion process, using

We thank Naresh Sharma, PhD. and Waruna Seneviratne for providing detailled information on the executed tests.

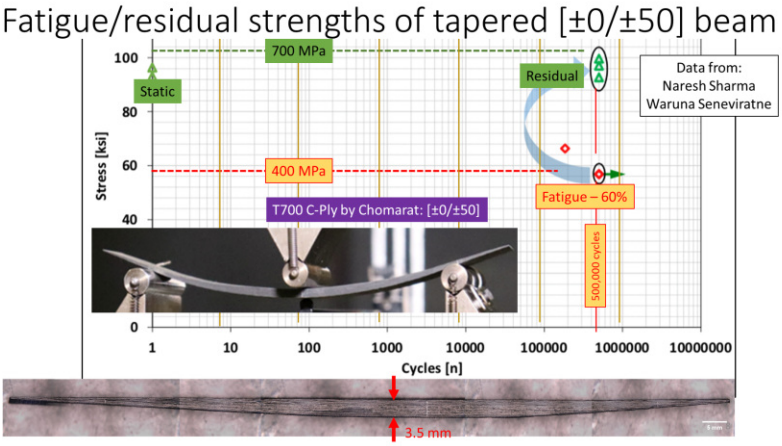

Figure 11: Fatigue testing of a tapered DD sample

Nashero's ZeroVoid Technology. The sample thickness is tapered, with a maximum thickness of 3.5 mm. The tested DD laminate features a $[\pm 0/\pm 50]$ building block, with the 0°-direction being aligned in the sample's length direction.

Note that complementary data for the tested material (Basis B properties) are provided in Chapter 4 of the 2019 book [2]

The green triangle data points corresponding to cycle 1 in Figure 11 on the left shows quasi-static strength results. The red diamonds indicate the fatigue specimens. The fatigue test specimens survived 500000 cycles at a stress level equal to 60% of quasi-static strength are indicated in red diamonds with a green arrow to the right. The residual strengths of these runouts are indicated in green triangles at 500000 cycles. These data indicate no residual strength degradation after 500.000 cycles.

Single-omega-stringer column

Vescovini et al. [8] examined a single-stringer column compression test numerically and experimentally. Figure 12 shows the examined geometry with the tapered stringer feet. The authors considered DD

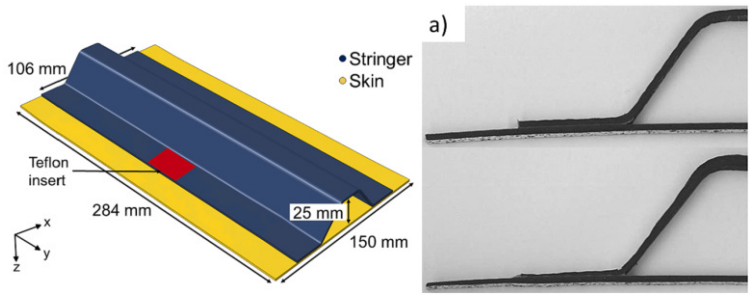

(a) Specimen dimensions (b) Tapered stringer shape

Figure 12: Numerically and experimentally examined single-stringer column. Figures extracted from [8]

laminates for skin and stringer, while the post-buckling behavior and

collapse were in focus of the study. The laminates are composed of two C-Ply™NCF types (T700 fibers), one with [+45/-45] and one with [30/-30] ply orientation. The laminates were manufactured with a low-viscosity epoxy matrix system in an out-of-autoclave process. Selected, concluding remarks are summarized hereafter.

- *'..it is noteworthy that the separation in the two tapered specimens progresses almost uniformly in the two flanges,'*
- *'These observations suggest that adopting DD stacking sequence, and exploiting the card sliding (see Section 5 in this article) manufacturing technique, can result in enhanced structural performance of composite structures'*

A DD 'flex-panel'

Kappel et al. [4] (Chapter 13) utilized the tapering opportunities of DD laminates to tailor the deflection curve of a DD panel in a displacement controlled cantilever scenario. Figure 13 shows the 'DD flex-panel' test stand, a corresponding FE model and the bottom side of the tapered DD sample, with eight different laminate thickness zones

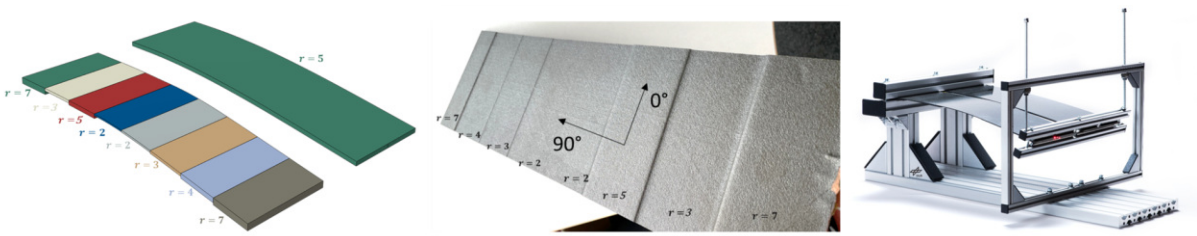

Figure 13: DD flex-panel demonstrator, FE model and tapered DD sample (bottom surface shown)

The samples are made from Hexcel's M21E/IMA medium grade UD prepreg. They were cured in an series-type autoclave process. The laminates feature $[0, 50, -50, 0]$ building block, which is a link to the prospected application in a high-lift device for a next-generation wing.

Optical full-field scans are used to digitize the deflected shape of the panels. Excellent match between those measurements and a corresponding FE model was found. Thus, the effect of locally adapting the number of building-block repeats on the deflection curve could be examined numerically. Figure 15 shows the comparison, between experiment and FE and selected tapering options, which underline the high level of design freedom for DD laminates.

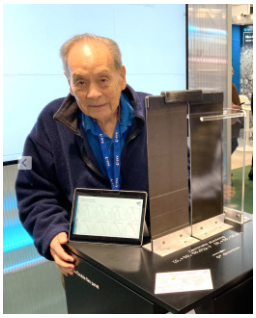

Figure 14: Steve Tsai, with the Double-Double flex-panel laminates at DLR booth at JEC 2024 in Paris

The study reveals valuable insight. The satisfying match between model predictions and the experiments paves the way for

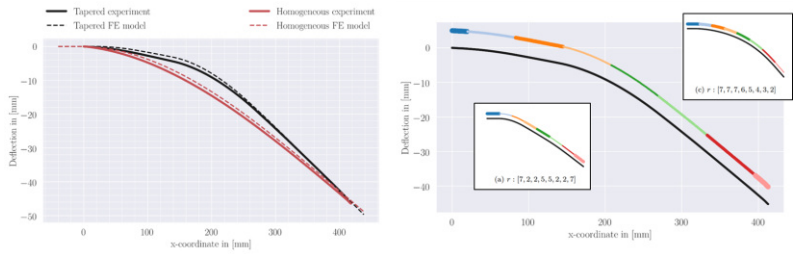

Figure 15: DD flex panel. Experiments vs. FEM (left), potential deflection shapes for different thickness variations (right)

the prospected application. Increasing the number of zone and the varying the zone dimension are additional design parameters which can be utilized in future application. Optimization was found comparably simple, as only inter-type problems need to be solves, which refer to the local number of building-block repeats.

Note, that the DD-flex panel demonstrator features integrated fiber-optical strain sensors along the bent. Results of those sensors, which are embedded at different levels of the laminate stacks, are examined in a related article [28].

ENF study

Neto et al. [33] present an experimental study on the end-notched flexure (ENF) behavior of DD and Quad laminates. The study is the first, which focuses on glass-fiber-reinforced plastics (GFRP) in DD context. The authors compare the Quad baseline $[45, 90, -45, 0]_{2s}$ with an $[A]$-equivalent DS laminate $[67.5, -22.5, 22.5, -67.5]_4$. Figure shows the 16 shows the examined samples. Figure 17 shows force-

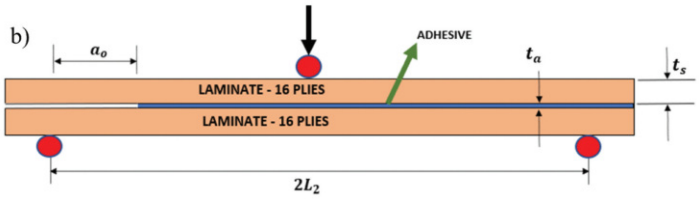

Figure 16: ENF sample with $2L_2 = 130$ mm, $a_o = 45$ mm, $t_a = 0.3$ mm, $t_s = 5.8$ mm

over-displacement graphs of the executed tests.

The authors conclude, that the *'Experimental results showed that DD laminates can significantly improve the shear fracture energy of adhesive joints and also delay the crack propagation over the test'*.

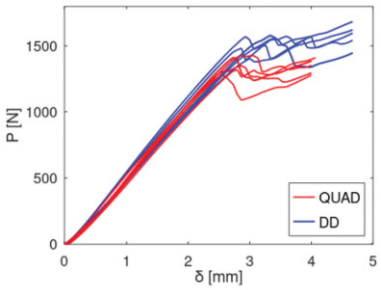

Figure 17: Force-over-displacement graphs for the ENF tests. Image from [33]

Other Studies

Vermes et al. [34] published a comprehensive article, which addresses the application of Tsai's modulus in context of laminate design for DD and Quad laminates. Figure 18 shows results laminates made from T700 C-Ply/M21, made in autoclave by Hexcel, tested by Alan Nettles. Figure 19 shows multiple results from multiple tests for a T700/epoxy laminate (exact resin not specified in [34]) provided by Toray America. The laminates are more orthotropic, which the Quad

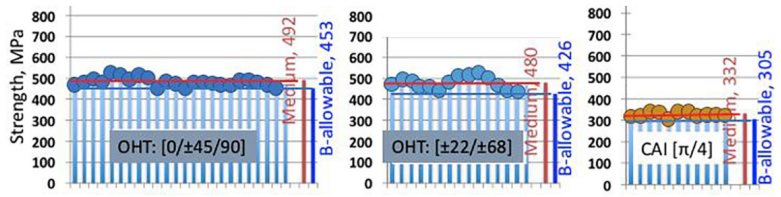

Fig. 15. Comparison of OHT and CAI between $[0/\pm 45/90]$ and $[\pm 22.5/\pm 67.5]$.

Figure 18: Test data, comparing Quad $[0/\pm 45/90]$ with the $[A^*]$-equivalent DD stacking $[\pm 22.5/\pm 67.5]$. Images from Vermes et al. [34]. Measurements executed by Alan Nettles

being a $[50\%, 40\%, 10\%]$ composition. Note, that more-orthotropic laminates are often denoted as 'hard' in DD context.

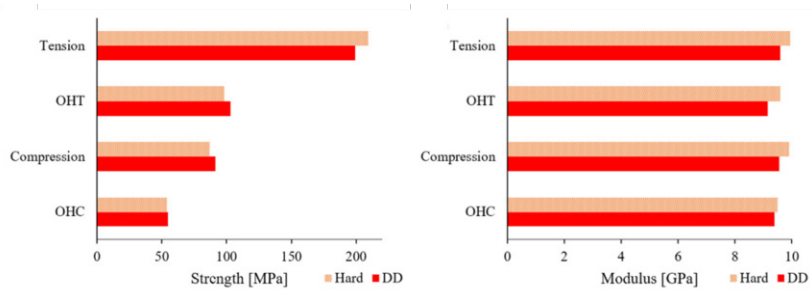

Figure 19: Test data, comparing a more-orthotropic Quad $[0_5/(\pm 45)_2/90]_s$ (denoted as 'hard') with the $[A^*]$-equivalent DD stacking $[\pm 0/\pm 50]_{5T}$. Images from Vermes et al. [34]

4 *Numerical studies*

Optimal DD laminates for multiple load cases

Kappel presented a study [14] on finding optimal DD laminates for different multi-load scenarios. Table 1 shows two selected load scenarios (N_i in MN/m), with five individual loads per case.

Case	Load	N_1	N_2	N_3	N_4	N_5
Fuselage	N_x	0.5	0.5	0.5	0	−0.1
	N_y	1	1	−0.1	1	1
	N_{xy}	0	0.2	0.2	0.2	0.2
Upper Wing	N_x	−1	−1	−1	0.2	0.5
	N_y	0	0.2	0.2	−0.4	0
	N_{xy}	0	0	−0.3	0	0

based on the definition of the strain threshold ST, as

$$ST = \varepsilon_x^2 + \varepsilon_y^2 + \gamma_{xy}^2/2 \tag{2}$$

The, formulation allows for directly determining the required number of building block repeats r, which is needed to not violate the

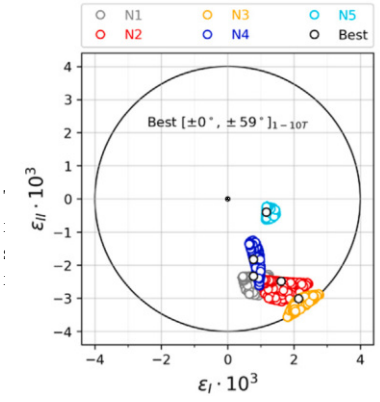

(a) Upper wing

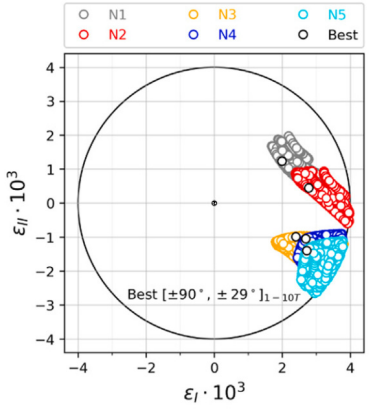

(b) Fuselage

Figure 20: Multi load visualization.

defined strain threshold. It is given by

$$r = \frac{\sqrt{\left(a_{11}^* N_x + a_{12}^* N_y\right)^2 + \left(a_{12}^* N_x + a_{22}^* N_y\right)^2 + \frac{\left(a_{66}^* N_{xy}\right)^2}{2}}}{4 \cdot t_{ply} \cdot ST} \tag{3}$$

with $[a^*] = [A^*]^{-1}$ being the inverse of the thickness-normalized in-plane laminate stiffness matrix $[A^*]$.

The ceil operation $r \rightarrow \lceil r \rceil$ is important to highlight, as full building block are a prerequisite for a DD laminate. The novel relations are used to determine a corresponding r-value for each load scenario of a case. As r directly refers to the minimum laminate thickness, the highest value need to identified from the individual load scenarios of a case. Thus, the minimum number of repeats for a group of loads is determined by $r_{min} = max([r_i])$. Figure 20 shows the results of the fuselage and the upper-wing cover scenario. The $[\pm 90, \pm 29]$ BB

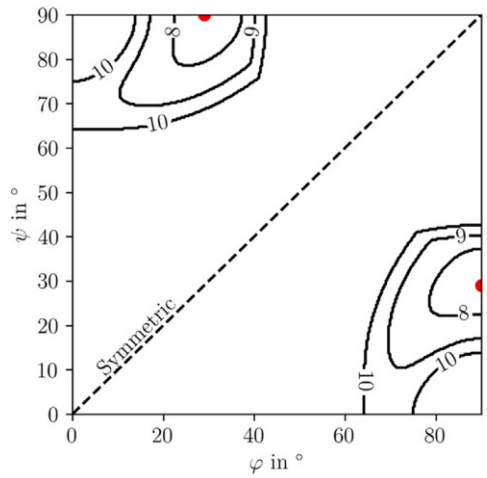

Figure 21: Minimum repeats over DD design space, for the fuselage scenario shown above

is determined for the fuselage case, while the $[\pm 0, \pm 59]$ BB is determined for the upper wing case. Figure 21 plots the minimum number of repeats iso-lines over the DD design space. The plot captures all five individual load scenarios of the case. It shows that the loads can by carried, when eight building block repeats are realized, leading to $[\pm 90, \pm 29]_{8T}$.

Space application

Guin and Nettles [5] examined a large-scale, adapter-type structure. Figure 22 shows the structure, which features a 5 m (15 ft) forward diameter, an 8.3 m (25 ft) aft diameter and a 45° cone angle (Thus 1.4 m (5 ft) height). They considered IM7/8552 UD, medium-grade prepreg for the cover sheets of the sandwich acerage. The acerage has

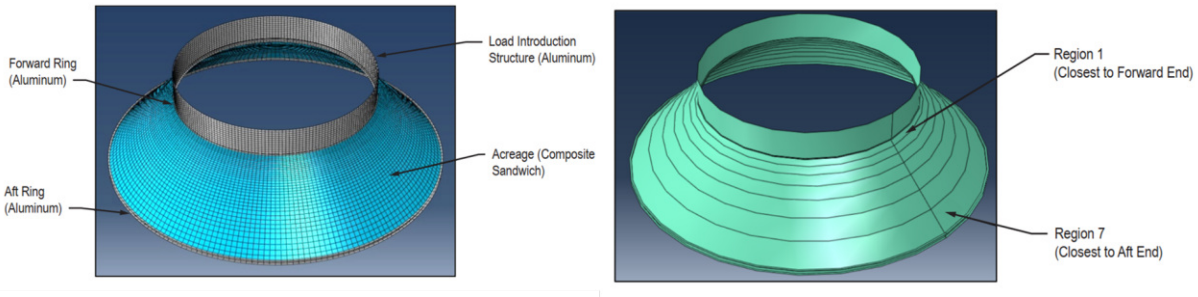

Figure 22: A large-scale, adapter-type structure examined by Guin and Nettles [5]

been subdivided in seven laminate zones. Guin and Nettles started with a $[+45/0/-45/90]$ baseline laminates. The competing laminate was $[\pm 25]$ layup, which is a DD special case, with $\varphi = \Psi$ (also denoted as single-double).

The essential results of the study are summarized hereafter.

- *'$[\pm\varphi]$ layups provide for improved thickness tailoring due to minimal effective repeating unit size'*
- *'While thickness tailoring can entail additional design complexity at/near transition regions, $[\pm\varphi]$ layups may provide for significant design flexibility even through the late stages of a project. '*
- *'The flexibility afforded by the minimal effective repeating unit size in $[\pm\varphi]$ layups, which may allow a composite structure to be readily adapted in light of design changes over the course of a project while minimizing weight and avoiding significant schedule and/or cost impacts, is seen by the authors to be the most significant practical benefit.'*

Wing box (generic)

Zerbst et al. [21] extended their Lightworks framework [25] for the consideration of DD laminates. The novel implementation has been applied to a tip-loaded generic wing box structure, which features upper and lower covers, ribs and spars. Both cover layups were subject to optimization, aiming for minimum weight- Laminate strength and buckling (compression & shear) criteria were considered. Figure 23 shows the generic wing-box shape.

The example is a reference case in contest of composite-laminate optimization (see [26, 27]). Zerbst et al. concluded:

- *Optimization of DD more efficient due to less amount of design variables and constraints*
- *Huge advances for DD due to manufacturability and easy refinement of the wing box design in later development phases*

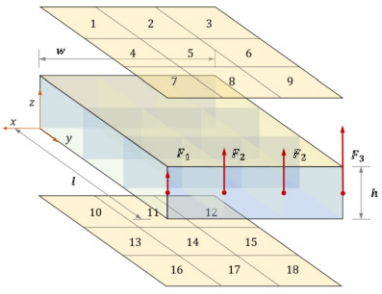

Figure 23: Generic wing box

Fuselage barrel

Garofano et al. [15] examined a complex fuselage structure numerically, which is subjected by a 5m drop height. Figure 24 shows the examined barrel, with a diameter of 3462 mm and a length of 1845 mm. The study focuses on the structural replacement of the conventional skin layup $[90, 45, 0, 45, -45, 90, 0, -45, 45, -45]_s$ (20%,60%,20%) with a DD substitute. The authors identified $[\pm 30, \pm 45]$ as the optimum DD replacement. The model distinguishes seven individual laminate regions, as shown in Figure 25.

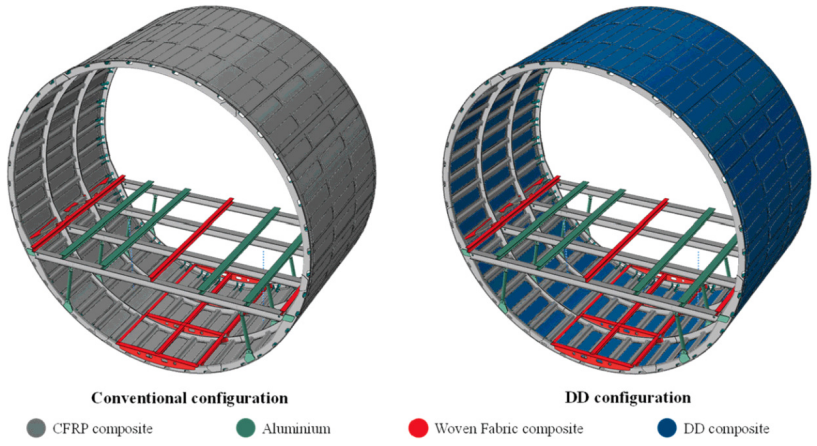

Figure 24: Complex fuselage FE model used for the study. Image from [15]

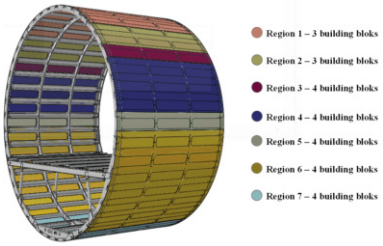

Figure 25: Individual laminate zones for the fuselage's outer skin. Image from [15]

Each zone can potentially feature an individual number of BB repeats. Garofano et al. consider strength requirements. The authors outline a skin mass reduction of 69.8%. The proposed DD configurations show a different, collapse behavior. The reader is referred to [15] for detailed discussion.

Wing cover

Shrivastava et al. [13] created a numerical study in context of aircraft wing panel optimization. The examined wing is related to the Suchoi Su-27 Flanker aircraft. Figure 26 shows the FE model, which composes three Spars, upper and lower covers as well as multiple ribs. The baseline laminate were developed from a 40-ply starting laminate $[(0, 90, \pm 45)_5]_s$.

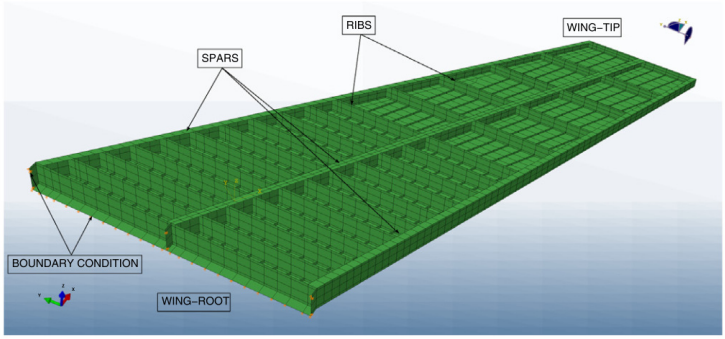

Figure 26: Examined wing FE model (upper cover not shown)

The authors determined a $[\pm 0/\pm 54]$ building block to substitute a more-orthotropic (65%,17%,18%) laminate and a $[\pm 13/\pm 65]$ building block for a (37.5%,37.5%,25%) laminate. The applied DD search process was set up in a conventional manner focusing on the laminate-thickness-normalized in-plane laminate stiffness matrix $[A^*]$, using the formulation: $Min : \sum |A^*_{ii,DD} - A^*_{ii,Quad}|$ for $i = 1, 2, 6$. Shrivastava et al. [13] assess thermo-elastic deformations for both the baseline structure (Quad) and their DD solutions. Figure 27 shows the comparison. The authors concluded that DD structures show less thermo-elastic distortion as structures made from conventional laminates, as $D^*_{16,26}$ are proportional to $1/r^2$. The authors outline 24% lower mass of the DD solution, compared to the structure made from conventional laminates.

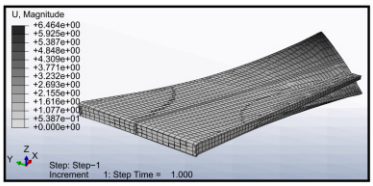

(a) Quad

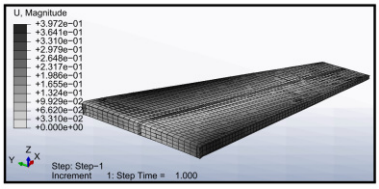

(b) DD

Figure 27: Thermo elastic deformations for $\Delta T = 128$°C, Scaled 150x. Images extracted from [13]

Integral C-profile fuselage frame

Doberts [6] examined whether DD laminates can offer potential benefits for C-profile integral fuselage frames. Figure 28 shows the utilized FE model. The baseline model features Quad laminates. The DD version in Figure 28 features seven laminate regions around the mouse hole of the frame. The study results are briefly outlined here-

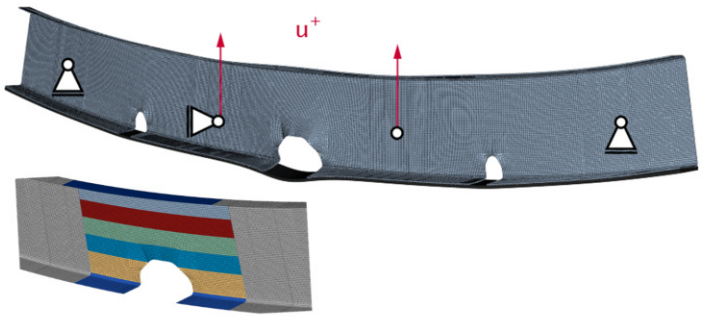

Figure 28: Examined four-point bending scenario with seven defined DD laminate zones around the mousehole region

after.

- *The homogenization criterion led to thicker laminates compared to the Quad baseline. Thin-ply laminates allows for weight reductions.*
- *As buckling was critical for the frame, mimicking Quad with DD replacements does not lead to weight reduction*
- *Numerical analysis, which allow for identifying the best DD angles, independent from pre-existing Quad laminates, promise weight savings, however at the cost of reduced stiffness, which suggest the consideration of additional constraints within the optimization process.*

In total, the study does dot reveal remarkable advantages for the examined frame structures. It should be kept in mind that those kind of structures often feature more-orthotropic laminates with 0° ply fraction $> 50\%$, which cannot be directly transferred to equivalent DD laminates.

Buckling of DD-laminate panels

Kappel [9] examined buckling of bi-axially loaded, simply-supported rectangular plates from a DD perspective. The independence of the relevant D^*_{ij} coefficients from the repeat parameters r was found the key to considerable simplification (see Equation 1).

$$r = \sqrt[3]{N_0 \cdot \frac{3a^2}{16\pi^2 t_{ply}^3} \cdot \frac{m^2+n^2}{D^*_{11}m^4 + 2\left(D^*_{12}+2D^*_{66}\right)m^2n^2 + D^*_{22}n^4}}$$
$$r \propto \sqrt[3]{N_0} \tag{4}$$

m, n denote half-wave numbers, a denotes the edge length of the quadratic panel (k=1) and t_{ply} denoted the ply thickness. The D^*_{ij} are the coefficients of the thickness-normalized stiffness matrix $[D^*]$.

Figure 29 shows an example graph. It can directly be determined analytically, based on the considered m-n cases The green area circumscribes all feasible laminate configurations, which can sustain the defined buckling load at minimum weight. The plot shows r-isolines. The number of repeats r is proportional to the panel mass (M), with $M = 4 \cdot t_{ply} \cdot a^2 \cdot \rho \cdot r$.

Kappel applied the results of [9] to a multi-panel scenario in [10]. The examined 18-panel use-case is also known as the 'horse-shoe' example and has bee proposed by Soremekun et al. in 2002 [23]. It represents a standard case, examined multiple studies on laminate blending, executed by different research groups. Figure 30 shows the problem description and the final DD result. DD's two-parameter

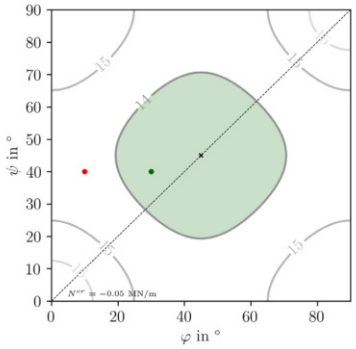

Figure 29: Minimum-weight DD laminates over the φ, Ψ design space.

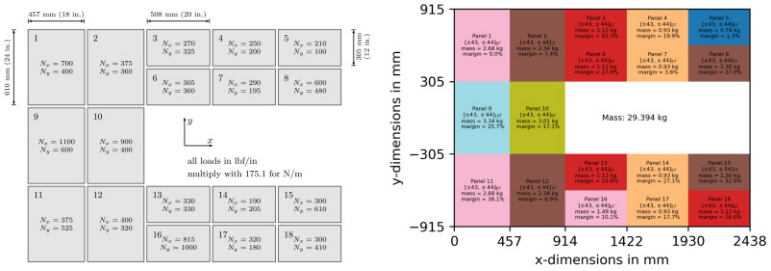

Figure 30: 'Horse-shoe' use case and DD optimum solution

design spaces allows for another interesting plot. Figure 31 plots the total mass of all blended 18 panels. The green region indicates the group of the lightest manufacturable panels.

DD optimum weight for the 18-panel scenario is found around 7.9% lighter compared to results of Shvarts and Gurarev, who examined conventional laminates made from $0,^\circ, \pm 45^\circ, 90^\circ$ plies. Other research groups presented slightly lighter optimum 18-panel set, but the regarded design spaces were incomparably larger.

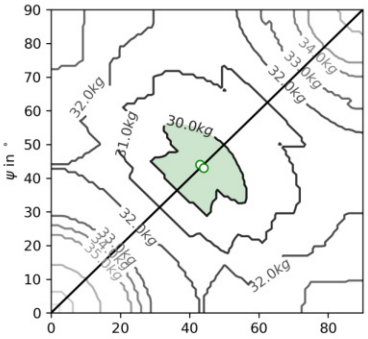

Weight	Source	Comment
29.39 kg	**DD configuration**	$[\pm\varphi, \pm\Psi]_{rT}$, full building blocks only, thus total plies always multiples of 4 (22 plies = infeasible)
31.89 kg	Shvarts and Gubarev [13]	Limited to $[0^\circ, \pm 45^\circ, 90^\circ]$ plies, considering industrial laminate design rules, as symmetry or 8% rule (among others)

Figure 32: Summary of the 18-panel buckling study

SLS study

A numerical study on single-lap joints has been published by Alves et al. [32]. The authors investigate the effect of exchanging and Quad baseline laminate $[45, 90, -45, 0]_{2s}$ by DD equivalents. with all varieties of the $[\pm 22.5, \pm 67.5]$ building block. All DD laminates fulfill the $[A]_{Quad} = [A]_{DD}$ condition. The study utilized material data for Hexply®6376C-HTS(12K)-5-35% Figure 33 shows the FE model for the SLS sample and a selected result, which shows the distribution of the $\sqrt{J_2}$ parameter which is defined as $\sqrt{J_2} = s_{ij}s_{ij}/2$, with $s_{ij} = \sigma_{ij} - (\sigma_{ij}/3)\delta_{ij}$ being the deviatoric stress tensor. The results in [32] indicate that all DD layups improve the joint damage onset, obtaining forces up to 25 % higher than for the equivalent Quad and smother transition of the stress invariants.

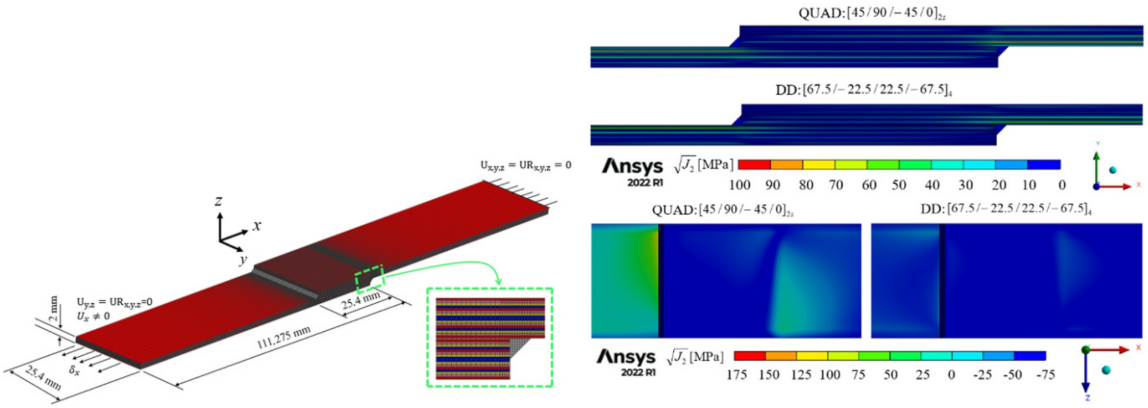

Figure 33: SLS sample and numerical results. Images from [23]

5 *DD's unique manufacturing opportunities*

Thickness tapering

The repeat index r determines the thickness of any DD laminate $[...]_{rT}$, as $t_{lam} = r \cdot 4 \cdot t_{ply}$. Thus, laminate-thickness changes refer to changing local BB repeats. The basic DD idea is to have full BB run-outs/ drop-offs.

In contrast, in conventional aerospace laminates, single ply drop-offs are common practice, which is related to the fact, that drop-offs are usually covered by continuous cover plies on both part surfaces. The basic DD approach allows for run outs on the outer part surfaces, as shown in Figure 34.

Figure 34: Building-block run outs/drop-offs on the upper part surface

Figure 35 shows an DD example structures. The panel-like component feature a local thickness increase from 3 to 10 repeats. The panel shows how DD laminates will look like when they are manufactured with single-sided toolings.

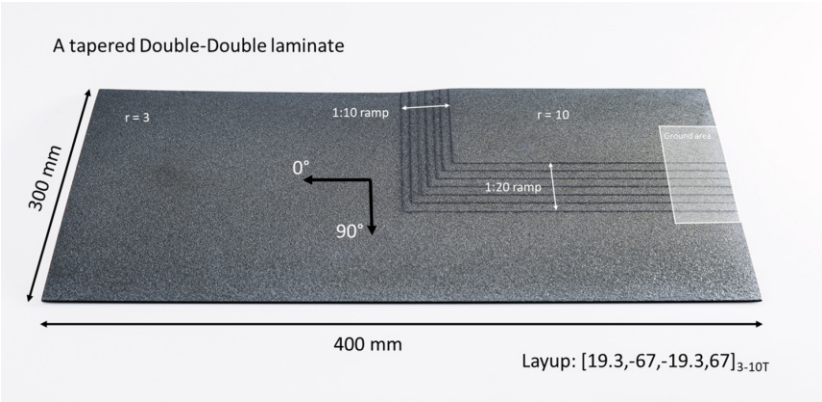

Figure 35: A prepreg-made DD panel, with a thickness transition from 3 to 10 building blocks (12 - 40 plies, 2.2 - 7.4 mm), 1:10 and 1:20 ramping

The part features an approximated 1:20 along the 90° -direction

and a steeper 1:10 ramp along the 0° direction.. BB run outs are located on the outer surface. The discrete stair-shaped architecture is smoothed during the autoclave process. The manufacturing concepts offer the opportunity to manufacture a three-BB base laminate and apply a pre-manufactured (and potentially trimmed) DD patch. Figure 36 shows an Ω-shaped profile, which shows a tapered part cross section. The stack of flat laminates is formed, using a single-sided

Figure 36: Cross-section tapered DD omega profile, card sliding, formed from a flat full-laminate ply stack of M21E/IMA UD prepreg

diaphragm process and cured afterwards on an aluminum tooling. The laminate thickness features zone with 1 up to 8 repeats. The part is made from eight flat building-block laminates of the same size. The laminate is composed, applying the 'card-sliding' technique presented later in this section

The border between tapering and patching dilutes. Tapering can be realized in longitudinal direction as well. The combination of longitudinal, transverse and local patching opens a huge design space for designers, which is dissimilar larger compared to conventional laminates. Figure 37 shows example for both options.

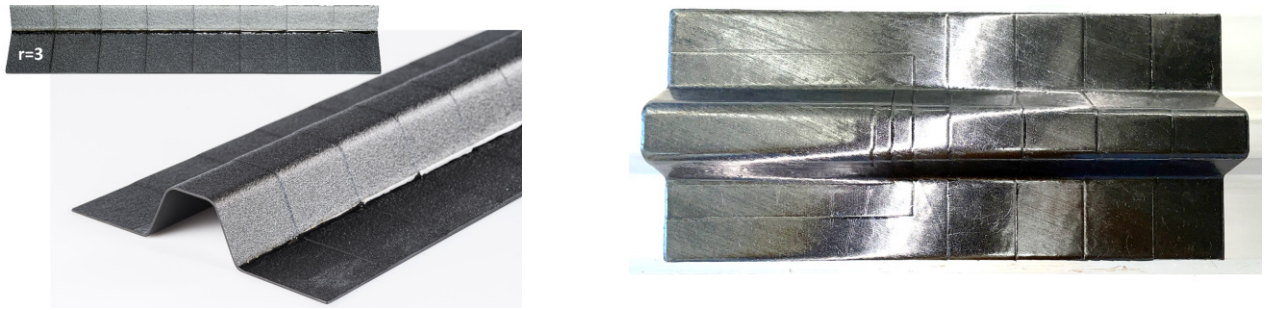

Figure 37: Tapering in the part's longitudinal direction (left) and an uncured laminate complex combination of longitudinal, cross-section tapering and local patching (right), All parts were formed from flat full-laminate ply stacks, M21E/IMA prepreg

Control surfaces in aerospace applications, such as flaps, flaperons and ailerons, are in focus for next generation of high aspect ratio wing for single-aisle aircrafts. Weight saving will be a key challenge for longer wings, in order not to overcompensate aerodynamic

advantage by too high wing mass. DD laminate can help to save weight, due to the absence of a 10% rule for example.

Figure 38 shows a DD laminate for a flap body. The skin is made from four building blocks with $[\pm 16, \pm 65]$ stacking. M21E/IMA prepreg is used and the skin is cured in an autoclave using an outer tool in a bladder manufacturing techniques. The prepreg preform

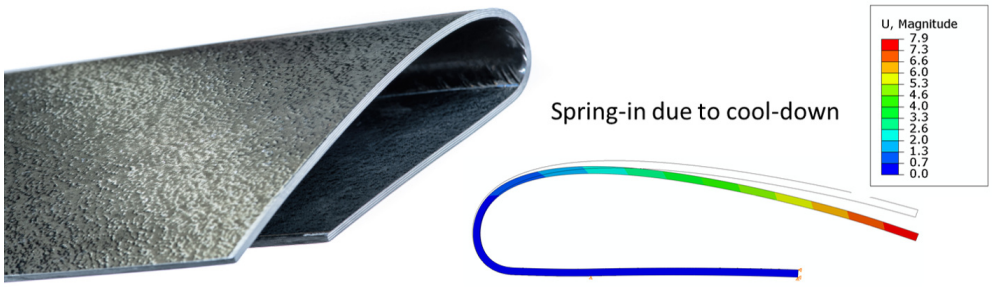

Figure 38: 16-ply (r=4) Flap, autoclave cured, made from M21E/IMA UD prepreg, with spring-in deformation prediction (in [mm]) for cool down from 180°C to 20°C.

has been created of a simple male-tool, while the laminate is created from flat BB laminates. Note, that similar spring-in characteristics are present for QUAD and DD, as the resin-dominated properties in laminate through-thickness direction remain.

Combining DD and Quad

In cases minimum laminate thickness shall be realized, the DD concept potentially can have some limitations. DD's 'homogenization' process requires a certain number of BB repeats in order to reduce the critical couplings in $[B]$ and $[D]$, Three to four repeats are recommended, which refers to 12-16 plies. For low-grade prepreg, with an approximate ply thickness of 0.125 mm, this leads to a minimum laminate thickness of 1.5 - 2.0 mm. Thin-ply materials ($t_{ply} = 0.08$ mm) can be used to achieve minimum laminate thicknesses of 0.96 - 1.28 mm. However, those materials are not established in today's series-type structures. This led to the question whether DD can be combined with a Quad base laminate. A test article has been realized to examine this point. An 8-ply QI Quad base laminate, from medium-grade prepreg is locally patched with three building block of a DD substitute with a $[22.5, -67.5, -22.5, 67.5]$ BB. Figure 39 shows the sample setup. The illustrated FE results (shell model in ABAQUS CAE), refer to a cool down study, which models a temperature step of -160K, referring to the cool-down after finishing the autoclave curing. The ply CTEs were set to $\alpha = 0$ ppm/K and $\alpha_2 = 33.0$ ppm/K. The deformation plot show deflections of 0.56 mm, for the 400 mm x 400 mm base laminate, with the 200 mm x 200 mm DD patch in the center. Figure 40 shows the cured

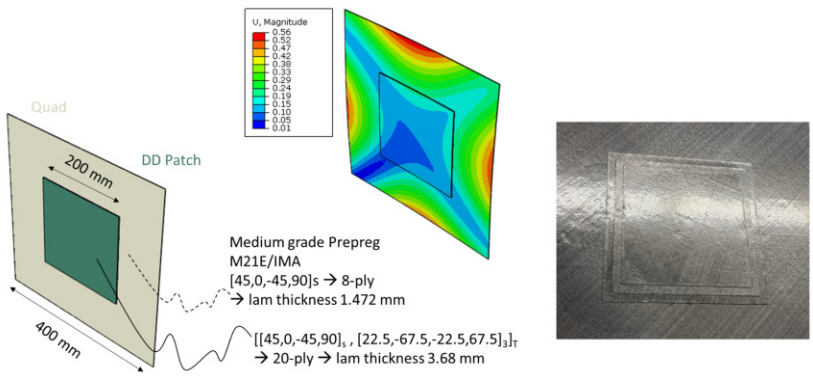

Figure 39: DD patch on Quad QI base laminate. Cool-down simulation and sample during manufacturing (uncured)

sample, which substantiates the numerical analysis. No warpage is observed, even though the center has a 20-ply, full asymmetric $[[45, 0, -45, 90]_s, [22.5, -67.5, -22.5, 67.5]_3]_T$ layup.

Patching a Quad base laminate with DD-patches locally also work for more-orthotropic laminates. Figure 41 shows a (50%/40%/10%) Quad base laminate, with is locally patched with a tapered, 3-repeat DD patch. The center-region laminate is described by the stacking $[[45, 0, -45, 0, 90]_s, [9.2, -61, 6, -9.2, 61.6]_3]_T$. The patch's building block has been determined on an $[A^*]$ basis. The parts shown in

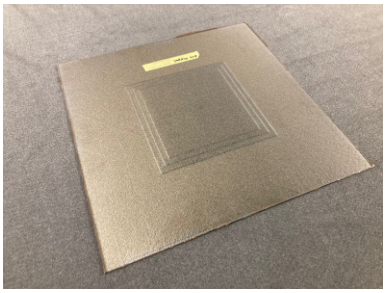

Figure 40: Cured sample with DD patch on QI base laminate, showing no relevant warpage

Figure 41: Patching a more-orthotropic (50/40/10) Quad laminate with $[A^*]$-matching DD patches

Figures 40 and 41 are made from series type Hexcel M21E/IMA UD prepreg. Patches are applied prior 180°C autoclave curing. Both parts show no relevant warpage after manufacturing, even though the laminate stackings are fully asymmetric in the patch region.

Card Sliding

The phrase 'card sliding' describes a manufacturing approach. The concept name refers to a deck of cards, which consists of numerous single elements of the same size. By pushing the deck of cards from one side it forms into a parallelogram shape. This scenario is transferred to the laminate creation process. Figure 42 shows a schematic.

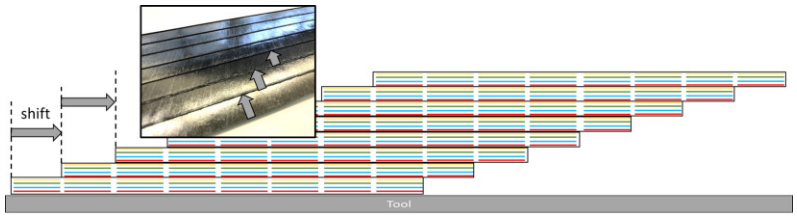

Figure 42: The principle of the 'card-sliding' concept

The four-coloured elements refers to a single building block of a certain size. In Figure 42, eight elements are stacking on each other. The 'parallelogram shape' is achieved by creating a shift between the individual BBs. This shift determines how the laminate taper looks like. In Figure 42 shows a constant shift, but this is no limitation. It can also be individual, ascending or decreasing.

'Card sliding' clearly benefits from DD's laminate architecture, which does not require laminate symmetry. It can be applied for profiles with tapered cross sections, as indicated in Figure 43, and re-

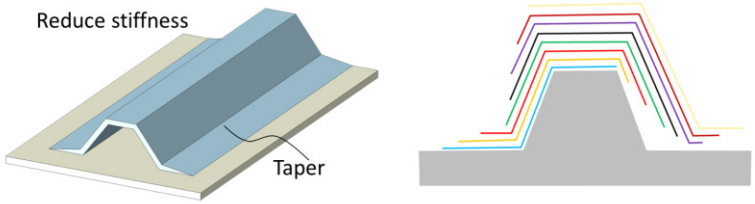

Figure 43: 'card-sliding' of tapered omega stringer. Left figure redrawn from [30]

alized for the Ω-profile in Figure 36. Card sliding has also be applied for the NCTE cylinder shown in Figures 47 and 46. It shall be noted, that the card-sliding concept creates a certain level of asymmetric. Figure 44 shows the bottom surface of the Ω-stringer, which has been manufactured with the card-sliding techniques.

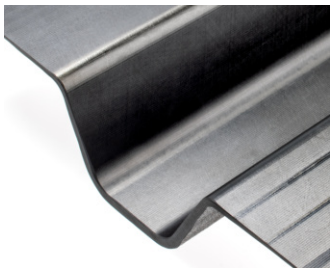

Figure 44: Bottom surface with BB run outs on the right flange

While run outs on one flange are located on the part's upper surface, run outs on the other flange a located on the tool side. Due to resin flow during the autoclave pressure the interface surface shows the usual excellent quality. However, whether those run-out region increase the risk for crack initiation, when the stringer is attached to a skin, requires examination. At the same time, the inner laminate architecture is free of resin-pockets at ply-drop offs, which can be a

beneficial aspect in term of crack initiation. Both topics need further attention.

Other profiles

Figure 45 shows as a generic fixed-leading edge part, which features a formed Double-Double laminate.

The D-nose structure has been realized for validation purposes of a novel manufacturing concept, which will be further matured in an upcoming research project. Structural cut outs will be examined and DD's patching opportunities shall be used, demonstrated and assessed.

Figure 45: D-nose trial, spring-in compensated

Special-purpose structure: NCTE Cylinder

CFRP Structures are known for their low thermal expansion. Analysis show, that some laminates, made from beta $[\varphi, -\varphi]$, lead to negative laminate CTE α_x and moderate laminate CTEs in transverse direction α_y. Figure 46 shows how the laminate in-plane CTEs change for varying φ with $\alpha_1 = 0.022$ ppm/K and $\alpha_2 = 28.0$ ppm/K.

Negative CTEs induce counterintuitive behaviour of structures. Heating leads to contraction and vice versa. The particular behavior

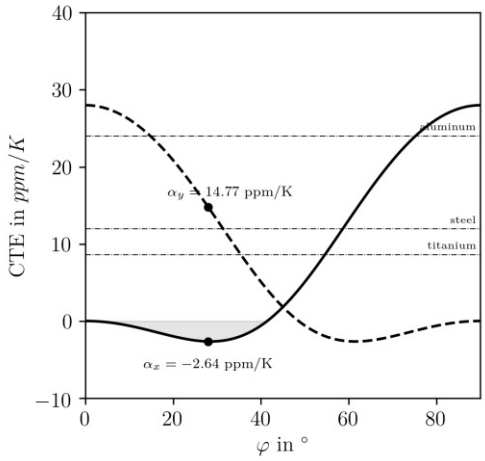

Figure 46: Negative CTEs (grey-marked region for CTE α_x) for some $[\varphi, -\varphi]_{rT}$ laminates

has been utilized for joining a metallic outer grid (wire-eroded) and an inner thick CFRP DD liner. The concept idea is to create a joint of both structure, which utilizes overlapping dimensional tolerance windows at room temperature. Figure 48 shows both independently manufactured parts. The outer part diameter of the CFRP tube exceeds the inner diameter of the grid. An assembly is not possible. Heating the inner CFRP component, induces a reduction of the tube radius. The CFRP tubes slit into the cold metal grid. The cooling

down of the CFRP tube, back to room temperature, leads to expansion, which is counteracted by the metallic grid. Tube and grid for a joint, but can also be separated by heating up again. It shall be

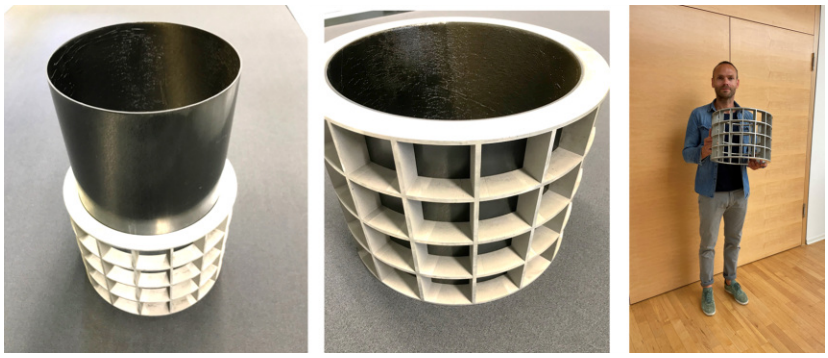

Figure 47: DD CFRP inner skin with negative CTE in circumferential direction. Allowing for a reversible assembly with a metallic grid, by heating the CFRP component. Grid received by DLR. Grid made and provided by Charles Zheng from Zhejiang University, China.

noted, that the presented example is only suited for below-room-temperature conditions. It shall also be noted, that heating up the metallic grid would also allows to the described assembly concept. However, the test with the heated CFRP liner has been executed to verify tool-compensation capabilities, as the exact diameter of the utilized aluminum tool required compensation, in order to account for the 180° curing temperature of the CFRP tube.

The presented tube has been roll-formed from a flat card-sliding stack. The shift length was design to avoid overlapping, which was essential for a constant-thickness tube. The concept of glueless joints is part of an initiated patent application [31]

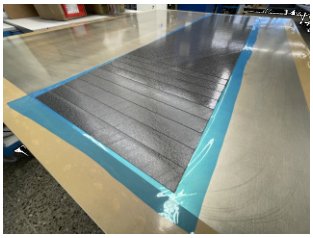

Figure 48: Card-sliding approach for the flat laminate, which is later rolled into the female tooling

Crash applications

Thickness tapering can be utilized aside from aerospace applications. DD's tapering opportunities can be interesting for crash-element applications. Figure 49 shows rather conventional crash elements, with constant material thickness and constant or changing cross sections. Figure 49 also shows novel concepts, which utilize local

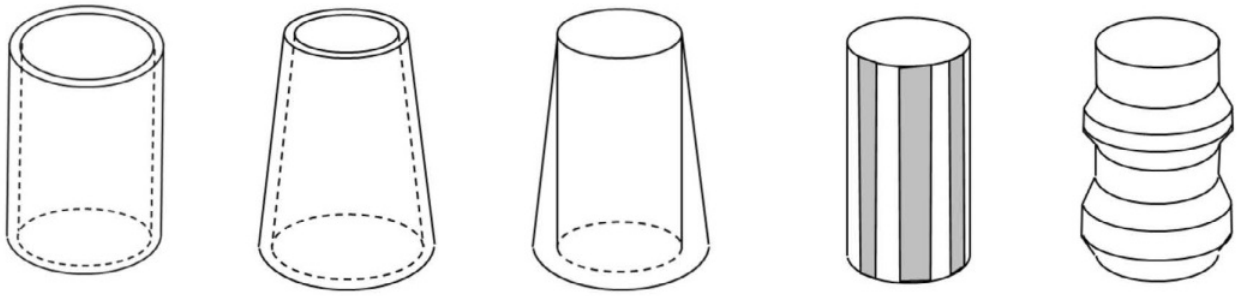

Figure 49: Conventional (1,2) crash elements and novel designs (3,4,5), enabled by DD's tapering opportunities. Figure from [4]

patches, which widen the design space for tailoring the structural characteristics to given demands.

How DD's BB drop-off regions look in reality

Quad laminate usually feature so-called cover plies, which cover ply run-outs/drop-offs, and lead to rather smooth laminate-thickness transitions. The basic DD laminate concept allows for building-block run outs on both part surfaces. Thus, 4-plies are dropped off at once.

Figure 50 shows a schematic for an CAI sample, with drop-offs on the upper surface. When such a DD sample is cured the effective

Figure 50: DD ramp schematic for a CAI sample

laminate architecture won't show the steps. The bagging arrangement, the acting autoclave pressure will lead to resin flow. Due to the resin movement, the upper surface will be smoothed after processing. This section examines the effective laminate shape of a cured DD laminate with four discrete BB drop-offs. The study, has accompanied the CAI study [11], which is summarized above in Section 3.

Optical scans using a GOM ATOS system have been used to measure the tapered Quad and DD samples. Figure 51 shows the generated data, which already indicate the different laminate architecture of the tapered regions for both laminate types. The data has been

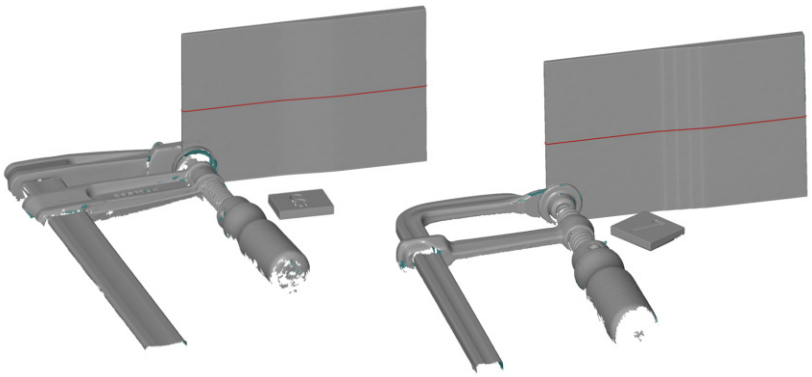

Figure 51: ATOS scan to assess effective ramp shapes. Red lines indicate the evaluated cross sections. See DD's discrete BB run outs on the right.

appropriately aligned within the GOM Inspect software and center-plane sections were created based on the tessellated point cloud (see red section cuts in Figure 51). The section-cut data sets have been exported for more detailed analyses using Python. Figure 52 shows the relevant excerpt (45-100 mm from the 125 mm long sample) of the generated section cuts around the ramp area and the nominal 1:10

ramp. The detail shows the effective laminate shape at a single BB drop-off. It can be seen clearly that the theoretical step-like shape is flattened out as a consequence of the combination of a single-sided tool and the autoclave procedure. The smooth shape of the Quad and

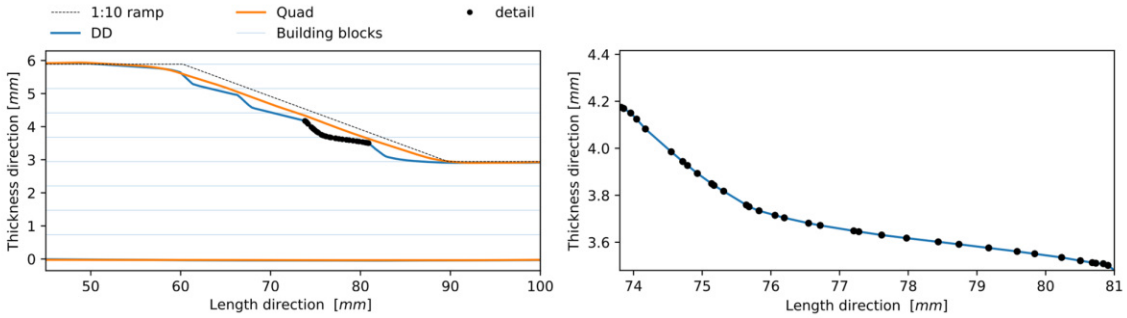

Figure 52: Full DD ramp section (left) and single drop-off detail (right)

the stepped shape of the DD laminate can be clearly seen. For DD, a single BB is composed of four plies, leading to a BB thickness of $t_{BB} = 0.736$ mm, leading to a step length of 7.36 mm, for the regarded 1:10 ramp and the nominal ply thickness of $t_{ply} = 0.184$.

The neat resin regions are examined. A parametric model has been deduced, which basis on the ply-thickness as the main parameter. The model allows for quantifying the effect, when DD laminates are made from thin-ply material, as it is often described. Figure 53b

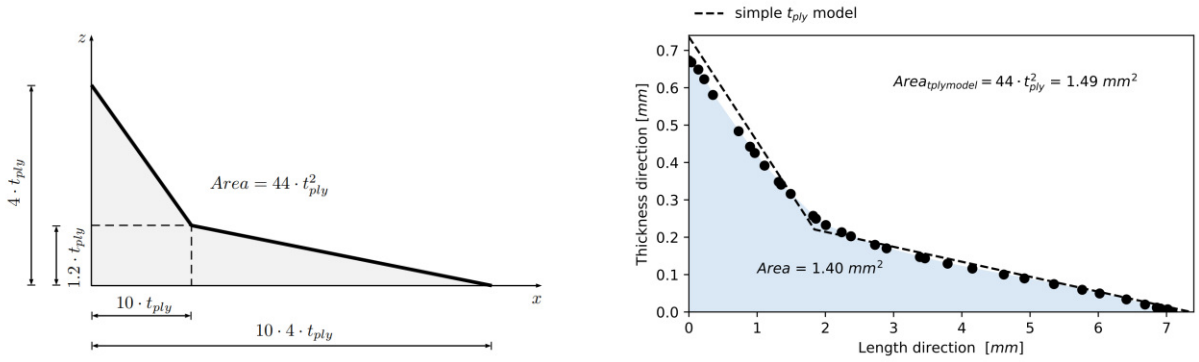

(a) Parametric model

(b) Application

Figure 53: Parametric model and effective neat resin area at BB drop off

shows the measured detail, the corresponding area (blue) and the model result. The analysis provides two main results:

- The neat resin area is proportional to t_{ply}^2. Thus, reducing the ply thickness to 25% of the initial thickness (0.184 mm $\rightarrow$ 0.046 mm) leads to 1/16 of the reference neat resin areas. As four thin-ply BBs replace a single reference BB, the effective neat-resin area is 1/4 of the reference, when a laminate with the same thickness is

examined.

- For the CAI sample at hand, with 4 BB drop-offs and a width of 100 mm, the total volume of neat resin is determined to $4 \cdot 100\ \text{mm} \cdot (44 \cdot 0.184^2)\ \text{mm}^2 = 596\ \text{mm}^3$, which is equivalent to 0.72 g neat resin, for an assumed resin density of 1.2 g/cm^3) .

6 Examined materials in DD context

The following table summarizes the materials (Prepreg, dry-fiber etc.), which have been examined in experimental studies.

Table 2: Materials used/examined in DD studies

Study	Source	Comment on material
CAI	[11]	Hexcel M21E/IMA UD prepreg, medium grade, autoclave cured
OHT		Hexcel M21E/IMA UD prepreg, medium grade and IM7/8552 UD prepreg low grade, both autoclave cured
NCTE barrels		Hexcel M21E/IMA UD prepreg, medium grade, autoclave cured
Tapered frames/ skin		Hexcel M21E/IMA UD prepreg, medium grade, autoclave cured
DD flap skin		Hexcel M21E/IMA UD prepreg, medium grade, autoclave cured
DD cone	[5]	IM7/8552 UD prepreg, medium grade, 35% resin content
Generic wing box	[21]	T300/N5208 UD prepreg, low grade 0.27 mm ply thickness
DD Stringer column	[8]	NCF C-Ply™thin-ply with 50 g/m^2 fiber-areal weight, Out-of-autoclave infusion with low viscosity ProSet INF 114/212 epoxy resin system
Tapered DD samples	[35]	0/50 C-Ply™, with 50 g/m^2 Toray's T700 fibers

7 A comment on 'Metalite'

In recent presentations at JEC 2024 [35] a laminate family called 'Metalite' has been proposed by Steve Tsai. The particular group has been initially found by Antonio Miravete. 'Metalite' is similar to the DD architecture and laminates, which explains why it presented in this article. The group of 'Metalite' laminates show unique properties, which are outlined hereafter. A 'Metalite' laminate is defined by an 8-ply building block

$$[[-\varphi,\varphi,\varphi,-\varphi],[\varphi,-\varphi,-\varphi,\varphi]]_r$$
$$[[+\varphi,-\varphi,-\varphi,+\varphi],[-\varphi,+\varphi,+\varphi,-\varphi]]_r \quad \text{(mirrored)},$$

with r being the repeat parameter, as known from DD laminate notation. Thus, when full building-blocks are used, the discrete laminate thicknesses $t_{lam} = 8 \cdot t_{ply} \cdot r$ can be realized. For a low-grade prepreg, with 1/8 mm ply thickness this means discrete millimeter steps.

In practice, designers strive for laminates which shall show a decoupled behavior, in particular no in-plane extension-shear coupling ($A_{16}, A_{26} = 0$), no bending extension coupling ($[B] = [0]$) and no/little bending-twist coupling ($D_{16}, D_{26} \approx 0$). Those 'decoupled' laminates show a rather simple mechanical behavior in terms of deformation characteristics. They behave similar as isotropic materials, such as aluminum for example. The corresponding ABD-matrix pop-

ulation in the classical-laminate theory (CLT) is shown on the right.

$$[ABD^*] = \begin{bmatrix} \bullet & \bullet & 0 & 0 & 0 & 0 \\ \bullet & \bullet & 0 & 0 & 0 & 0 \\ 0 & 0 & \bullet & 0 & 0 & 0 \\ 0 & 0 & 0 & \bullet & \bullet & 0 \\ 0 & 0 & 0 & \bullet & \bullet & 0 \\ 0 & 0 & 0 & 0 & 0 & \bullet \end{bmatrix}$$

For conventional 'Quad' laminates, this particular matrix population is achieved when the established stacking conventions (known as 'stacking rules'), such as mid-plane symmetry and the $\pm$ ply 'balance' are followed. For Double-Double laminates, this population is approached when the number of building-block repeats $r \gg 1$ increases, which leads to homogenization. 'Metalite' laminates, inherently show this matrix population without, any 'repeat' requirement. The following section shows why.

A 'Metalite' laminate:

- is composed of a single $(r = 1)$ or a group $(r > 1)$ of 8-ply sublaminates, where each sublaminate consists of two symmetric, but mirrored 4-ply building blocks
- is described by a singe ply angle φ.
- is fully asymmetric.
- always balanced

The last characteristic bullet directly explains the in-plane decoupling ($A_{16}, A_{26} = 0$). The other decoupling mechanisms require a more in-depth analysis of the $[B^*]$ and $[D^*]$ matrix entries, which are defined as

$$[B^*] = \frac{2}{t_{lam}^2} \cdot \frac{1}{2} \sum_{k=1}^{n} [\bar{Q}]_k (h_k^2 - h_{k-1}^2) = \frac{1}{t_{lam}^2} \cdot \sum_{k=1}^{n} [\bar{Q}]_k (h_k^2 - h_{k-1}^2)$$
$$[D^*] = \frac{12}{t_{lam}^3} \cdot \frac{1}{3} \sum_{k=1}^{n} [\bar{Q}]_k (h_k^3 - h_{k-1}^3) \quad .$$

A particular characteristic of the global ply stiffness $[\bar{Q}]$ matrix is the key to achieve decoupling. The matrices are provided hereafter for a $+\varphi$ and a $-\varphi$ ply.

$$[\bar{Q}_\varphi] = \begin{bmatrix} \bar{Q}_{\varphi,11} & \bar{Q}_{\varphi,12} & \bar{Q}_{\varphi,16} \\ \bar{Q}_{\varphi,12} & \bar{Q}_{\varphi,22} & \bar{Q}_{\varphi,26} \\ \bar{Q}_{\varphi,16} & \bar{Q}_{\varphi,26} & \bar{Q}_{\varphi,66} \end{bmatrix} \ , \ [\bar{Q}_{-\varphi}] = \begin{bmatrix} \bar{Q}_{\varphi,11} & \bar{Q}_{\varphi,12} & -\bar{Q}_{\varphi,16} \\ \bar{Q}_{\varphi,12} & \bar{Q}_{\varphi,22} & -\bar{Q}_{\varphi,26} \\ -\bar{Q}_{\varphi,16} & -\bar{Q}_{\varphi,26} & \bar{Q}_{\varphi,66} \end{bmatrix} \tag{5}$$

One observes, that the coefficients $\bar{Q}_{11,22,12,66}$ are independent from the ply-angle sign. The $\bar{Q}_{16,26}$ coefficients, in contrast, change sign when the ply-angle sign changes. This sign dependency of the $\bar{Q}_{16,26}$ coefficients is elegantly utilized in the 'Metalite' context to realize uncoupling of in-plane and out-of-plane effects. The matrices $[B^*]$ and $[D^*]$ are composed of ply-specific contributions. Those contributions are basically defined by the terms $h_k^2 - h_{k-1}^2$ and $h_k^3 - h_{k-1}^3$,

respectively, wherein h_k and h_{k-1} denote the plies' top- and bottom-surface z-coordinate (see Nettles [29]). Table 3 outlines those specific contributions for the eight plies in the 'Metalite' building block.

Ply	h_k	h_{k-1}	$h_k^2 - h_{k-1}^2 = 2 \cdot h_k \cdot t_{ply} - t_{ply}^2$	$h_k^3 - h_{k-1}^3$
8	$4 \cdot t_{ply}$	$3 \cdot t_{ply}$	$7 \cdot t_{ply}^2$	$37 \cdot t_{ply}^3$
7	$3 \cdot t_{ply}$	$2 \cdot t_{ply}$	$5 \cdot t_{ply}^2$	$19 \cdot t_{ply}^3$
6	$2 \cdot t_{ply}$	$1 \cdot t_{ply}$	$3 \cdot t_{ply}^2$	$7 \cdot t_{ply}^3$
5	$1 \cdot t_{ply}$	$0 \cdot t_{ply}$	$1 \cdot t_{ply}^2$	$1 \cdot t_{ply}^3$
4	$0 \cdot t_{ply}$	$-1 \cdot t_{ply}$	$-1 \cdot t_{ply}^2$	$1 \cdot t_{ply}^3$
3	$-1 \cdot t_{ply}$	$-2 \cdot t_{ply}$	$-3 \cdot t_{ply}^2$	$7 \cdot t_{ply}^3$
2	$-2 \cdot t_{ply}$	$-3 \cdot t_{ply}$	$-5 \cdot t_{ply}^2$	$19 \cdot t_{ply}^3$
1	$-3 \cdot t_{ply}$	$-4 \cdot t_{ply}$	$-7 \cdot t_{ply}^2$	$37 \cdot t_{ply}^3$

Table 3: Ply-specific, location-dependent contributions to $[B^*]$ and $[D^*]$

One observes two types of 'contribution symmetry'. For the $[B^*]$ matrix, it is characterized by an additional sign change for contributions above and below the laminate mid plane, which explains why symmetric laminates always show a [B]-matrix equal to zero. Table 4 shows how those symmetries are combined with the aforementioned sign characteristic of $[\bar{Q}]$. The columns distinguish between the 11, 22, 12, 66 matrix entries and the 16, 26 entries, as those two groups show different characteristics. When the sum of the

Ply	angle	Ply contributions to $[B^*]$		Ply contributions to $[D^*]$	
		$\bar{Q}_{11,22,12,66}$	$\bar{Q}_{16,26}$	$\bar{Q}_{11,22,12,66}$	$\bar{Q}_{16,26}$
8	$+\varphi$	$+7 \cdot t_{ply}^2 \bar{Q}_{11,22,12,66}$	$+7 \cdot t_{ply}^2 \bar{Q}_{16,26}$	$+37 \cdot t_{ply}^3 \bar{Q}_{11,22,12,66}$	$+37 \cdot t_{ply}^3 \bar{Q}_{16,26}$
7	$-\varphi$	$+5 \cdot t_{ply}^2 \bar{Q}_{11,22,12,66}$	$+5 \cdot t_{ply}^2 (-\bar{Q}_{16,26})$	$+19 \cdot t_{ply}^3 \bar{Q}_{11,22,12,66}$	$+19 \cdot t_{ply}^3 (-\bar{Q}_{16,26})$
6	$-\varphi$	$+3 \cdot t_{ply}^2 \bar{Q}_{11,22,12,66}$	$+3 \cdot t_{ply}^2 (-\bar{Q}_{16,26})$	$+7 \cdot t_{ply}^3 \bar{Q}_{11,22,12,66}$	$+7 \cdot t_{ply}^3 (-\bar{Q}_{16,26})$
5	$+\varphi$	$+1 \cdot t_{ply}^2 \bar{Q}_{11,22,12,66}$	$+1 \cdot t_{ply}^2 \bar{Q}_{16,26}$	$+1 \cdot t_{ply}^3 \bar{Q}_{11,22,12,66}$	$+1 \cdot t_{ply}^3 \bar{Q}_{16,26}$
4	$-\varphi$	$-1 \cdot t_{ply}^2 \bar{Q}_{11,22,12,66}$	$-1 \cdot t_{ply}^2 (-\bar{Q}_{16,26})$	$+1 \cdot t_{ply}^3 \bar{Q}_{11,22,12,66}$	$+1 \cdot t_{ply}^3 (-\bar{Q}_{16,26})$
3	$+\varphi$	$-3 \cdot t_{ply}^2 \bar{Q}_{11,22,12,66}$	$-3 \cdot t_{ply}^2 \bar{Q}_{16,26}$	$+7 \cdot t_{ply}^3 \bar{Q}_{11,22,12,66}$	$+7 \cdot t_{ply}^3 \bar{Q}_{16,26}$
2	$+\varphi$	$-5 \cdot t_{ply}^2 \bar{Q}_{11,22,12,66}$	$-5 \cdot t_{ply}^2 \bar{Q}_{16,26}$	$+19 \cdot t_{ply}^3 \bar{Q}_{11,22,12,66}$	$+19 \cdot t_{ply}^3 \bar{Q}_{16,26}$
1	$-\varphi$	$-7 \cdot t_{ply}^2 \bar{Q}_{11,22,12,66}$	$-7 \cdot t_{ply}^2 (-\bar{Q}_{16,26})$	$+37 \cdot t_{ply}^3 \bar{Q}_{11,22,12,66}$	$+37 \cdot t_{ply}^3 (-\bar{Q}_{16,26})$
		$\Sigma = 0$	$\Sigma = 0$	$\Sigma > 0$	$\Sigma = 0$

Table 4: Individual and summed ply-specific contributions to $[B^*]$ and $[D^*]$

ply-specific contributions is examined, one sees how the combination of 'contribution symmetry' and the sign-dependency of $\bar{Q}_{16,26}$ leads to an cancel-out effect of in the sum of specific contributions. One observes that $B_{ij} = 0$ and $D_{16,26} = 0$ is achieved, which explains how 'Metalite's particular laminate architecture, with the $[+\varphi, -\varphi, -\varphi, +\varphi, -\varphi, +\varphi, +\varphi, -\varphi]$ building block, realizes a fully decoupled laminate characteristic.

A first manufacturing trial, with Steve Tsai's proposed angle selection $\varphi = 20°$, for highly directed load scenarios, proves that a 'Metalite' part neither shows manufacturing induced warpage nor twist, which is a consequence of complete uncoupling. It will be interesting to see how 'Metalite' laminates will be used in the future!

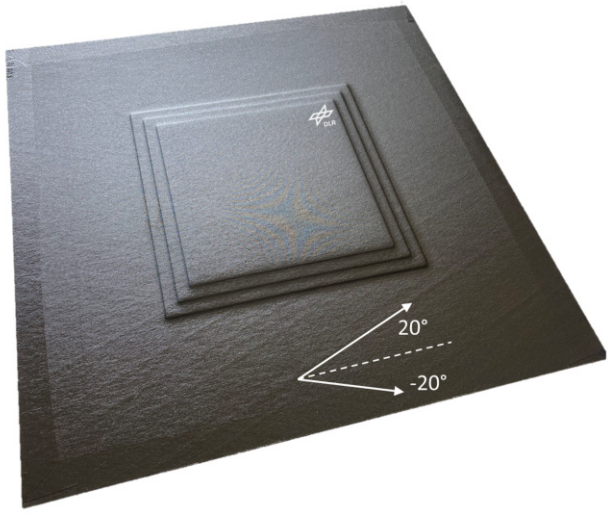

Figure 54: A 'Metalite' panel with $\varphi = 20°$, with local patches that neither shows asymmetry-induced warpage nor twist. Nominal thickness between 1.47 mm and 5.88 mm.

8 *Summary & Conclusion*

The present article provides a timely overview on published studies, on the family of Double-Double laminates. The particular DD group has been proposed by Steve Tsai in 2021 [1], as a promising challenger for the family of conventional laminates used in aerospace-practice over years.

DD laminates can be handled using the established classical laminates plate theory, which is used for conventional laminates for decades. A DD laminate features four discrete ply orientations, similar as conventional laminates. However, due to the balanced building block architecture $(\pm\varphi, \pm\Psi)$ a DD laminate can be described by only the two angles φ and Ψ. This represents a simplification and allows for elegant yet helpful illustration options.

The article presents pure numerical studies as well as studies with experimental focus. Considerable advantageous are prospected for DD in context of manufacturing. Therefore, selected manufactured components are presented, which demonstrate unique manufacturing opportunities (multi-dimensional tapering, card sliding, NCTEs), which are enabled by DDs particular BB-based laminate architecture.

The following bullet points briefly summarize selected highlights.

- Experimental studies (CAI, OHT,...) neither show remarkable advantageous nor disadvantageous for DD compared to QUAD. In this context, it should be noted that most often DD samples were designed to mimic existing Quad samples. In future studies it will be important to define DD laminates based on given loads independently from a Quad reference, in order to benefit from the free ply-angle selection. Mimicking Quad with DD will likely

not lead to remarkable improvements. However, when DD's design space is fully utilized, considerable advantageous are more likely (Numerical studies indicate it). The combination of Quad and DD, in a fuselage context for example, pursues the ambition to *'combine the best of both worlds'*. A QI base laminate allows for minimum thickness, with an eight ply (1.47 mm with medium grade prepreg) laminate, which is critical to achieve with DD, as the homogenization requires a certain minimum BB repeats to get rid of coupling effects. The thin Quad base laminate, however, can be locally patched with $[A^*]$-compatible DD patches to increase the thickness locally, around cut-outs for example.

- Experimental studies, such as the presented CAI campaign show clear differences between Quad and DD. Impact-induced delamination differ, which as a consequence of difference of the fiber orientations. However, compression-after-impact tests show no direct correlation between total-delamination width and observed strength values. So far, manufacturing demonstrators and also the tapered CAI samples show BB run outs on the surface. This, artifact need additional attention to assess whether it creates risks for damage initiation. Fatigue testing is recommended. The effect of cover layers in DD laminates also need attention, whether those can affect the delamination characteristics relevantly.

- Selected numerical studies prospect considerable weight savings for DD-replacements of Quad reference structures. Mass reductions of over 69% for a fuselage-skin component [15]. and similar savings for a Wing-box, fuselage or a stiffened panel are presented [35]. Those prospected savings are surprisingly high, when it is considered that established materials (prepregs etc.) are considered. It will be essential, in the near future, to incorporate the industrial perspective into those studies, in order to substantiate whether the high savings, can be achieve for series-type structures.

- *'Simplification of design and manufacturing processes'* is considered a remarkable advantage for DD, even though *'simplification'* is a difficult parameter to quantify. However, it is linked to effort reduction and the shortening of development and manufacturing phases, which is an important cost driver. The presented multi-panel buckling case is a good example. It demonstrates that interdependence between adjacent laminate zones diminish for DD, as a consequence of the absence of the symmetry requirement. The definition of laminate transition zones simplifies drastically, as all zones of a DD structure feature the same building block only. Laminate thickness tapering is another interesting aspect of DD. Adapting

the local thickness, in patch-like manner becomes simplified, as the necessity to realize zone-to-zone compatibility is fulfilled per definition.

Figure 55 finally summarizes new design opportunities. I shows that conventional QUAD laminates can be combined with matching DD laminate patches. The combination can be interesting for repair scenarios or for fuselage laminates, when minimum laminate thickness is important. Figure 55 also shows, that DD can be made with

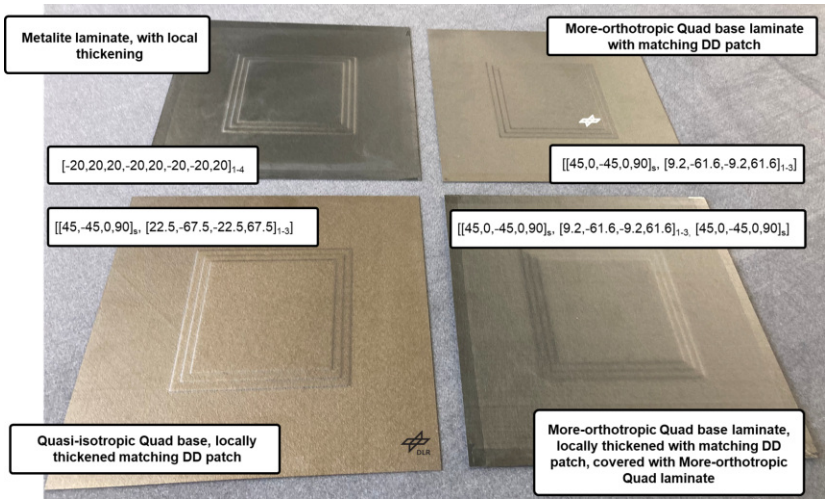

Figure 55: Examples for combining conventional QUAD base laminates with local DD laminate patches, for quasi-isotropic and more-orthotropic laminates, without or with cover plies. All combinations do not show warpage or twist, even though local stackings are fully asymmetric, as highlighted by the provided stacking sequences.

cover layers. All parts in Figure 55 are made from medium grade M21E/IMA prepreg and autoclave cured. None of the parts show warpage or twist.

Acknowledgements/Funding

Author Erik Kappel acknowledges: The project '101101974—UP Wing is supported by the Clean Aviation Joint Undertaking and its members. Funded by the European Union.

Views and opinions expressed are however those of the author only and do not necessarily reflect those of the European Union or Clean Aviation Joint Undertaking. Neither the European Union nor the granting authority can be held responsible for them.

Support

The authors appreciate valuable support from Waruna Seneviratne, PhD (National Institute for Aviation Research (NIAR), Wichita State University), Naresh Sharma, PhD (NASHERO) and Dr. Alan Nettles.

References

[1] Tsai SW. Double–Double: New Family of Composite Laminates. AIAA JOURNAL Vol. 59, No. 11, November 2021

[2] Tsai SW, Sharma N, Arteiro A, Roy S, Rainsberger B. Composite Double-Double and Grid/Skin structures. Low Weight/ Low Cost Design and Manufacturing International Paris Air Show, 2019

[3] Tsai SW et al. DOUBLE–DOUBLE A New Perspective in The Manufacture and Design of Composites. Stanford University, 2023

[4] Tsai SW et al. DOUBLE–DOUBLE Simplifying the Design and Manufacture of Composite Laminates. Stanford University, 2023

[5] Guin WE and Nettles AT. A Straightforward Approach to Thickness Tailoring in Composite Structures Using Non-traditional Layups NASA/TM–20210021062, Marshall Space Flight Center, Huntsville, Alabama, 2021

[6] Doberts AC. Application of an Innovative Design Approach to an Aircraft Frame Using Double-Double Laminates. Master Thesis. Hamburg University of Aplied Science. 2022

[7] Kappel E. On stacking-sequence independent bending properties of Double-Double laminates – A short communication. Composites and Advanced Materials Volume 33;1-5, 2024

[8] Vescovini A, Li CX, Mendez JP,d, Jin BC, Manes A, Bisagni C Post-buckling behavior and collapse of Double-Double composite single stringer specimens Composite Structures 327, 117699, 2024

[9] Kappel E. Buckling of simply-supported rectangular Double–Double laminates. Composites Part C: Open Access 11,100364, 2023

[10] Kappel E. On the Double-Double laminate buckling optimum for the 18-panel 'horse-shoe' reference case. Journal of Composite Science 8;77, 2024

[11] Kappel E, Boose Y, Mißbach M. A CAI study on transition zones of conventional and Double-Double laminates. Composites Part C: Open Access 14;100450, 2024

[12] Cunha RDd, Targino TG, Cardoso C, Ferreira EPdC, Junior RCSF and Melo JDD Low velocity impact response of non-traditional double-double laminates. Journal of Composite Materials, 2023

[13] Shrivastava S, Sharma N, Tsai SW, Mohite PM. D and DD-drop layup optimization of aircraft wing panels under multi-load case design environment. Composite Structures 248, 112518, 2020

[14] Kappel E. Double–Double laminates for aerospace applications — Finding best laminates for given load sets Composites Part C: Open Access 8, 100244, 2022

[15] Garofano A, Sellitto A, Acanfora V, Caprio FD, Riccio A. On the effectiveness of double-double design on crashworthiness of fuselage barrel. Aerospace Science and Technology Volume 140, 108479, September 2023

[16] Kappel E, Völkerink O, Boose Y, Kosmann Jens. An OHT study for Double-Double laminates made from 8552/IM7 and M21E/IMA low and medium-grade prepregs. Publication in 2024

[17] Kappel E. More-orthotropic Double-Double laminates? On the effect of adding additional plies to DD laminate building block. Publication in 2024

[18] Waruna Seneviratne Wichita State (ATLAS). Provided document. 2024

[19] Chromarat. C-PLY™Composites Reinforcements `https://composites.chomarat.com/en/brand/c-ply/`, 2024

[20] Tsai SW. A new laminate theory: simplified, invariant and universal Aeronautics & Astronautics,Stanford University NAFEMS, https://www.nafems.org/publications/resource_center/w_dec_23_global_2_p/, December 2023

[21] Zerbst D, Tönjes L, Ückert C, Dähne S, Werthen E, Kappel E and Hühne C. Gradient-based design optimization of composite structures using Double-double laminates. EASN Conference | 05.09.2023 - Salerno

[22] Tsai SW and Melo JDD. Composite Materials Design and Testing - Unlocking Mystery with invariants. Stanford University, 2015

[23] Soremekun G, Gürdal Z, Kassapoglou C, Toni D. Stacking sequence blending of multiple composite laminates using genetic algorithms. Composite Structures 56, 53-62 2002

[24] Erik Kappel. DD-laminates and manufacturing. Presentation Composites Design Workshop XXI, Stanford Aeronautics &Astronautics. 2021

[25] Zerbst D, Dähne S and Hühne C. Lightworks - MDO of a Composite Aircraft Wing. NRC22 NAFEMS Dach Regional Conference, Bamberg, 2022.

[26] Seresta O, Gürdal Z, Adams DB, and Watson LT. Optimal design of composite wing structures with blended laminates. Composites Part B: Engineering, 38(4),469–480, 2007

[27] Liu D, Toroporov VV, Querin OM and Barton DC. Bilevel Optimization of Blended Composite Wing Panels. Journal of Aircraft, 48(1), 107–118,2011.

[28] Kappel E, Boose Y, Prussak R and Kosmann J. On measuring laminate strains of a bent tapered Double-Double panel – Comparing strain data from an FE calculation, a high-resolution 3D camera system (ARAMIS) and a fiber-optical sensor system (FOSS). DLR-Interner Bericht. DLR-IB-SY-BS-2023-113. Open source, https://elib.dlr.de/199302/, 2023

[29] Nettles AT. Basic mechanics of laminated composite plates - NASA reference publication 1351. Technical report, NASA, 1994.

[30] Da Silva LFM et al. Design Rules and Methods to improve Joint Strength. Handbook of Adhesion Technology. Springer

[31] Tsai et al. Grid Structures having glueless sleeve joints and methods of manufacturing and using the same.United States Patent Application Publication. Pub. No.: US 2023/0234325 A1, 2023

[32] Alves GC, Vignoli LL and Neto RMC. Damage onset in CFRP single lap joint for DD and QUAD laminates Journal of Mechanical Science and Technology 38,1, Springer,2024

[33] Neto RMC, Vignoli LL, Moreira CS, Rohem NR and Sampaio EM Increase of shear fracture energy of adhesive joints using double-double laminates The Journal of Adhesion, 2024

[34] Vermes B, Tsai SW, Riccio A, Di Caprio S, Roy S. Application of the Tsai's modulus and double-double concepts to the definition of a new affordable design approach for composite laminates. Composite Structures 259, 113246, 2021

[35] Stephen W. Tsai and Antonio Miravete. Metalite. A new class of DD: stronger than steel, lighter than aluminum Presentation, JEC 2024, Paris, 6th March, 2024

[36] AITM 1-0007. Determination of plain, open hole and filled hole tensile strength. AITM norm, 2016

[37] Arteiro A, Sharma N, Melo JDD, Ha SK, Miravete A, Miyano Y, Massard T, Shah PD, Surajit R, Rainsberger R, Rother K, Cimini Jr. C, Seng JM, Arakaki FK, Tay T, Lee WI Sihn S, Springer GS, Roy A, Riccio A, Di Caprio F, Shrivastava S, Nettles AT, Catalanotti G, Camanho PP, Seneviratne W Marques AT, Yang HT, Hahn T. A case for Tsai's Modulus, an invariant-based approach to stiffness. Composite Structures 252; 112683, 2020

[38] Kappel E. On invariant combinations of Q_{ij} coefficients and a novel invariant I_Q. Composites Part C: Open Access 10; 100335, 2023